UNIVERSIDAD SAN FRANCISCO DE QUITO USFQ

Colegio de Ciencias e Ingenierías

Spaser Instability in Gain-Assisted Silver Nanoshell.

Proyecto de investigación

Andrés Cathey Cevallos

Física

Trabajo de titulación presentado como requisito
para la obtención del título de Licenciatura en Física.

Quito, 12 de mayo de 2016

UNIVERSIDAD SAN FRANCISCO DE QUITO USFQ

COLÉGIO DE CIENCIAS E INGENIERÍAS

HOJA DE CALIFICACIÓN
DE TRABAJO DE TITULACIÓN

Spaser Instability in Gain-Assisted Silver Nanoshell.

Andrés Cathey Cevallos

Calificación:

Nombre del profesor, Título académico: Alessandro Veltri, Ph.D.

Firma del profesor: _____

Quito, 12 de mayo de 2016

Derechos de Autor

Por medio del presente documento certifico que he leído todas las Políticas y Manuales de la Universidad San Francisco de Quito USFQ, incluyendo la Política de Propiedad Intelectual USFQ, y estoy de acuerdo con su contenido, por lo que los derechos de propiedad intelectual del presente trabajo quedan sujetos a lo dispuesto en esas Políticas.

Asimismo, autorizo a la USFQ para que realice la digitalización y publicación de este trabajo en el repositorio virtual, de conformidad a lo dispuesto en el Art. 144 de la Ley Orgánica de Educación Superior.

Firma del estudiante: _____

Nombres y apellidos: Andrés Cathey Cevallos

Código: 00109215

Cédula de Identidad: 1714769013

Lugar y fecha: Quito, 12 de mayo de 2016

Resumen

Se realiza un estudio teórico del acople entre la resonancia plasmónica de un nano-cascarón de plata y la emisión de un material activo dentro del nano-cascarón bombeado externamente. Para estudiar los campos eléctrico y de densidad de polarización se utilizó la aproximación quasiestática (válido para partículas de radio menor a $\sim 15\ [nm]$). Con el formalismo de optical-Bloch se hizo la descripción de la interacción del momento dipolar de los elementos activos y el campo eléctrico externo, al igual que la inversión de población de los elementos activos. El problema electromagnético para el nanocascarón acoplado con la dinámica de elementos activos fue resuelto en varios regímenes dinámicos y de estado estable. Una inestabilidad tipo spaser se observó luego de una cantidad umbral de material activo ($\varepsilon_h''(\omega_{21}) = -0.526$) tanto con un campo eléctrico externo aplicado y sin él. Esta inestabilidad resultó en una amplificación extremadamente fuerte para el campo eléctrico fuera del nano-cacarón que decae con la distancia como r^{-6}. La marcada localización del campo fuera del nano-cascarón, y la naturaleza de la evolución temporal de la intensidad de amplificación y de la inversión de población justifican llamar a este efecto un spaser.

Abstract

A theoretical study of the coupling between the plasmon resonance of a silver nanoshell and the emission of an externally pumped active medium inside the nanoshell is made. In order to study the system's electric and polarization density fields, the quasistatic approximation was used (valid for particles with radius $\sim 15\ [nm]$). The optical-Bloch formalism was used to describe the gain elements' dipole moment interaction with the electric field and their population inversion. The electromagnetic problem for the filled nanoshell particle coupled to the gain population dynamics was solved in several dynamic and steady-state regimes. A spaser instability is observed after a threshold amount of gain ($\varepsilon_h''(\omega_{21}) = -0.526$) both with an impinging external electric field, and in its absence. These instabilities translate to an extremely strong amplification of the outer field intensity, that decays with the distance as r^{-6}. The strong spatial localization of the field, and the temporal evolution of the intensity amplification and the population density justify calling this effect a spaser.

Agradecimientos

Gracias a Alessandro y a Ashod por guiarme en el proceso investigativo que resultó en este escrito. Espero que esto sea sólo el inicio. A Alessandro en particular por su infinita paciencia.

Gracias a mis compañeros y amigos - Ramiro, Harold, Sosa, Jorges, Wilsons, Raq, Chance, Camilo, Anto, Caro, Pableinz, Stefan, Joaquín, Pancho, y a los que falten de la M105!

A mis profesores - Darío, Carlos, Vincent, Edgar, et al.

Gracias a mis padres, Alan y Mónica, por apoyarme. A mi hermano por inspirarme. A toda mi familia.

Y a Paula por darme fuerza - sin tí se hubiera demorado hasta el verano.

Para quien la lea completa.

Contents

Derechos de Autor **3**

Agradecimientos **6**

1. General Introduction **10**
1.1 The Rise of Nanotechnology 10
1.2 Plasmonics 11
1.3 Spaser 11
1.4 Aim 12

2. Plasmonics **13**
2.1 Overcoming the Diffraction Limit 13
2.2 Surface Plasmons 15
2.3 Localized Surface Plasmons 17
2.4 Loss-Compensation 20
2.5 Surface Plasmon Amplification by Stimulated Emission of Radiation (SPASER) . 21

3. Theory **22**
3.1 Doped Metallic Nanoshell 22
3.1.1 Gain Material 22
3.1.2 Metal 24
3.2 Nanoshell and Gain Polarizability 25
3.2.1 Boundary Conditions 27
3.3 Time Dynamical System of Equations 27
3.3.1 Recovering the Classical Polarizability 28

4. Results **30**
4.1 An Experimentalist's Dream or: Fewer Gain for Thinner Shells 30
4.2 Instabilities for Zero External Field and Spasing Threshold 32
4.3 External Field Amplification - Linear Regime 34
4.4 Gain Depletion - Non-Linear Regime 36
4.5 Temporal Evolution: Non-Linear Regime 38
4.6 Conclusions 40

A. Density Matrix and Optical-Bloch Equations **41**
A.1 The Density Matrix (in the flesh) 42
A.2 Optical Bloch 44
A.3 Gain Permittivity 46

B. Classical (Steady State) Polarizability 48
B.1 Nanoshell Multipolar Model 48

Bibliography 52

List of Figures

1.1 Lycurgus Cup. . . . 11
1.2 Stained glass window. . . . 12

2.1 STED microscopy. . . . 14
2.2 Surface Plasmon Polariton propagating along a metallic surface. . . . 15
2.3 Surface Plasmon Polariton excitation 16
2.4 Nanosphere in host medium. . . . 17
2.5 Silver nanoparticle polarizability. . . . 19
2.6 Permittivity of host medium. . . . 20

3.1 Nanoshell geometry. . . . 22

4.1 Thickness dependency. . . . 31
4.2 Eigenvalues. . . . 33
4.3 Eigenvalues for $\hbar\omega = 3.0128$. . . . 33
4.4 Maximum Intensity Position. . . . 34
4.5 Exponential Intensity Amplification: Linear Regime. . . . 35
4.6 Linear Regime. . . . 36
4.7 Non-Linear Regime. . . . 37
4.8 Non-Linear Regime (two peaks). . . . 38
4.9 Intensity in time. . . . 39
4.10 Intensity in time (two peaks). . . . 39

A.1 Two-level atom. . . . 44

B.1 Nanoshell geometry. . . . 48
B.2 Nanoshell dipole. . . . 51

Chapter 1

General Introduction

1.1 The Rise of Nanotechnology

In 1959 Richard P. Feynman planted the conceptual seed that resulted in the beginning of *nanotechnology*[1] during his renowned talk "*There is Plenty of Room at the Bottom*". After his ideas of storing huge amounts of information in a very small scale became stilled in the minds of scientists, important achievements in nanotechnology emerged. Such as the invention of the scanning tunneling microscope (STM) in 1981 (that earned its creators the Nobel Prize in Physis in 1986), or the discovery of fullerenes around 1985 (Nobel Prize in Chemistry in 1996) [2–4]. This resulted in even more attention paid towards the field, and since the 2000's nanotechnology obtained scientific, commercial, and even political awareness.

Research on nanotechnology has managed to find its way into many different areas, including commercial applications. Consumer products such as straighter-flying golf balls, stiffer tennis rackets, antibacterial socks with silver nano-particles are now in the market [5]. Examples of nanotechnology in research include medical applications that are under study or in use such as extremely localized drug delivery systems [6], cancer detection through nano-carriers [7], and blood purification with magnetic nano-particles [8]. Highly symmetrical nano-tubes with high electron mobility (around $10\ [nm]$), have been used to create transistors of the MOSFET type [9, 10], thus improving the field of nano-electronics [11]. The possibility for optical quantum computing, that would allow exponentially faster calculations, is another field of research at the moment [12]. By making use of quantum dots (semiconductor nanoparticles), considerable reduction in size for spectrometers has been theorized by MIT scientists [13].

Yet another of the applications of nanotechnology lies within the field of computers. Probably the first achievement of nanotechnology in this field was a considerable improvement on the storage capacity on hard drives. The 2007 Nobel Prize in Physics was given to Albert Fert and Peter Grünberg for the discovery of *Giant Magnetoresistance*, which, when applied to the read heads of hard disks, lead to larger memory in hard drives [14]. Nano-optical computing promises considerable improvements to speed and memory. At the moment, transfer of information from one storage device to another is managed with both light and electrons. The premise of nano-optical computing lies in implementing photons throughout all the process. This would allow for considerable improvements in speed and a reduction in energy consumption [15]. This is considered to be achievable through nanophotonic technology in the transistor level [16].

[1] The National Nanotechnology Initiative (founded in 2000) provided a general description for nanotechnology: "science, engineering, and technology conducted at the nanoscale, around 1 to 100 nanometers" [1].

1.2 Plasmonics

The study of interactions between free electrons in metal and electromagnetic fields at the nanoscale is known as *Plasmonics*. Branching out from the broader field of nanophotonics, plasmonics is a "rapidly growing field of nanoscience concerned with the control of optical radiation on the subwavelength scale" [17]. The rapid expansion of this field has been driven mainly by the wide range of applications that it promises - "solar cells, high-resolution microscopy, drug design and many more" [16]. Recently, improved photovoltaic devices have been achieved through the use of plasmonics, thus permitting a reduction in the thickness of the cells [18]. Additionally, superlenses have been created via the excitation of surface plasmons, allowing for sub-diffraction limit observations [19, 20].

Although the main advances in plasmonics and its applications have occurred during the 21^{st} century, its fundamental elements - surface plasmons[2] and localized surface plasmons[3] - were described around the 1900s [16, 23]. Furthermore, we can trace the use of localized surface plasmons back to Roman times. One of the finest examples of this is the Lycurgus cup, fig. 1.1, that is characterized by a special type of glass (often called "ruby glass") [24]. This glass exhibits a peculiar characteristic: when a source of light is outside the cup, the glass is seen in a yellowish olive green tone. On the other hand, when the light is inside the cup, it displays a crimson red tone.

Studies of the Lycurgus cup discovered nanometric impurities made of gold, silver, and other elements inside the glass. The gold and silver nanoparticles were found to be the main elements for the behaviour described [25]. Golden nanoparticles are also the reason for some of the coloring of tainted glass windows, as was shown in 1904 by Maxwell-Garnett, fig. 1.2 [23].

FIGURE 1.1: Lycurgus cup (4^{th} century).

1.3 Spaser

An additional application of plasmonics was suggested in 2003 by Bergman and Stockman, who theorized the *spaser*: a quantum amplifier of surface plasmons through the use of stimulated emission of radiation. The spaser is an equivalent of a laser, but with SPs rather than photons [26]. It has been theorized that using a nanodevice of metal/dielectric composite medium

[2] Surface Plasmons (SPs) are coherent resonant oscillations of conduction electrons present in the interface between a metal and a dielectric in response to an incident optical field [21, 22].

[3] Localized Surface Plasmons (LSPs) are SPs confined in a nanoparticle [21].

FIGURE 1.2: Troyes Cathedral Stained Glass, France (14^{th} century)

a strong, coherent, field appears in a region smaller than the exciting wavelength [27]. In order to obtain a spaser-like response, compensation on the losses due to the metal need to be made. This is usually done with the use of pumped gain material (quantum dots, fluorescent molecules, dye of different lanthanids).

Spasers are proposed to be sources of optical fields from a nanometrical scale, but their applications are so vast that could potentially represent for the 2020's a technological revolution comparable, if not superior, to what the invention of the laser meant for the 1970's. Some of these applications would include advances in nanotechnology such as nanoscale lithography, probing and microscopy [28].

1.4 Aim

The aim of this work is to theoretically study the plasmonic response of a metallic nanoshell with an externally pumped active gain material (dye, quantum dots, fluorescent molecules) able to couple with the plasmon resonance (LSP). Exciting the nanoshell with an external probe field, and the gain material with a pump external field at a different frequency, a rich variety of regimes arise for different amounts of gain.

By studying the stimulated emission of radiation of the active medium, modeling the metal as a Drude metal, and considering a multipolar model for the polarization and the electric fields, three time dynamical equations are obtained and solved numerically. The results show a considerable amplification in the external field, as well as a stable, oscillatory, nature of the intensity amplification of the field outside the nanoshell. This response could be interpreted as a stable spaser emission on the outer surface of the metallic nanoparticle.

Chapter 2

Plasmonics

2.1 Overcoming the Diffraction Limit

In 1873, Ernst Abbe noticed a fundamental limit in the resolution of optical imaging instruments given by the diffraction of light [29]. Abbe found that it was only possible to observe objects smaller than roughly one half of the wavelength of the light used. Setting λ as the wavelength of the incident light, η the index of refraction of the medium used, and θ the angle of incidence, Abbe approximated the diffraction limit of a microscope as:

$$d = \frac{\lambda}{2\eta \sin\theta}$$

Formally, a resemblance between the diffraction limit and Heisenberg's uncertainty principle exists. Since the wave-vector of the incident light gives the momentum, $p_x = \hbar k_x$, and the wave-vector is inversely proportional to the wavelength, it is possible to obtain a relation between the uncertainty in position to the wavelength. In fact, in the unidimensional case this is expressed as eqn. 2.1. From this it follows that eqn. 2.2[1] (where Δx is the uncertainty in the position of an object under observation, and λ is the wavelength of the light used) sets a diffraction limit that is similar in magnitude to that found by Abbe [17].

$$\hbar \Delta k_x \, \Delta x \geq \frac{\hbar}{2}, \quad \text{where} \quad \Delta k_x = \frac{2\pi}{\lambda} \quad \text{is the maximum spread of } k_x. \tag{2.1}$$

$$\Delta x \geq \frac{\lambda}{4\pi} \tag{2.2}$$

Abbe's constraint means that for visible light ($\lambda \sim 500\ [nm]$) the diffraction limit does not allow for anything smaller than roughly $200\ [nm]$ to be observed. If this uncertainty is on the same order of the object's size, then an optical instrument cannot observe it, regardless of the instrument's quality. "Recently, however, several new exciting approaches in imaging have emerged that can *break* this rule under certain circumstances" [30].

In 1999, Thomas A. Klar and Stefan W. Hall achieved focusing below the diffraction limit through STED microscopy (stimulated emission depletion), which uses two laser fields, Fig. 2.1. A near-UV pulse excites fluorophores and a spatially offset pulse quenches all fluorescent response excluding a nanometric volume through stimulated emission [31,32]. Hall was awarded,

[1] For real lenses a correction based on the numerical aperture must be made.

together with Eric Betzig and William Moerner (who created a method to obtain a layered imaging scheme through detection of single fluorescent molecules), the 2014 Nobel Prize in Chemistry for the use of fluorescent molecules to surpass the diffraction limit. Other methods for either "shrinking" (confocal microscopy) or overcoming (near-field microscopy) the diffraction limit have been developed [33]. Using these, nano-optics attempts to work beyond the diffraction limit due to mayor technological applications such as "super-resolution microscopy or ultra-high-density data storage" [17].

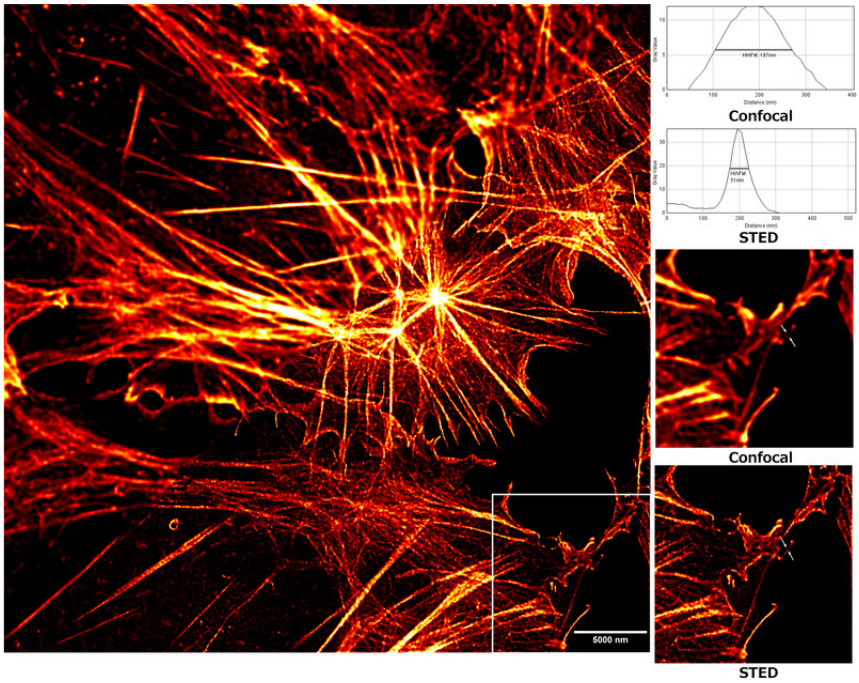

FIGURE 2.1: A figure showing the resolution improvement between traditional confocal microscopy and stimulated emission depletion (STED) microscopy. Cells were stained with 647-phalloidin to show actin filaments and the images were taken on a Leica SP5 2P STED microscope. Howard Vindin (2013), Wikimedia Commons

As is shown in eqn. 2.1, the spatial confinement of an object is given exclusively by the spread of the wave-vector in a given direction. This means that by increasing the spread of the wave-vector the spatial confinement of the object is lowered. This can be done by considering a tridimensional wave-vector, and increasing one of the perpendicular components of the wave-vector, e.g. $\hat{\boldsymbol{x}}$ and $\hat{\boldsymbol{z}}$, to a value larger than $2\pi/\lambda$ (e.g. $k_x \geq 2\pi/\lambda$), and at the same time making the other perpendicular component of the wave-vector to be purely imaginary (e.g. $k_z \in \Im$). This also maintains the requirement that the total length of the wave-vector, $k = \sqrt{k_x^2 + k_y^2 + k_z^2}$ is equal to $2\pi/\lambda$. By increasing the wave-vector in $\hat{\boldsymbol{x}}$, the spread in said direction is also increased, thus overcoming eqn. 2.2. However, this mathematical *trick* that cleverly allows the diffraction limit to be surpassed has a physical consequence. By introducing this imaginary component to the equation for a plane wave, eqn. 2.3 will describe the wave in the z direction. For positive z this means an exponentially decaying field, an evanescent wave, and for negative z it means an exponentially increasing wave - which has no physical meaning, hence it can be discarded [17].

$$e^{i\,k_z\,z} = e^{-|k_z|\,z} \tag{2.3}$$

This is the theoretical foundation that lays in the core of nano-optics, and the previously described evanescent wave will prove to be key for technologies such as near-field spectroscopy, or sub-diffraction limited superlenses [19,34,35]. Additionally, confocal fluorescence microscopy is a fundamental tool in biomedical research, and it also stretches Abbe's diffraction limit [17]. Slowly replacing it, is multiphoton microscopy, that was put forth by advances in nonlinear optics [36].

Another method for focusing below the diffraction limit of light is the use of surface plasmons, since they too fulfill the mathematical *trick* that was described. This is because surface plasmons are waves that show an evanescent decay on a metal-dielectric interface. From Maxwell's macroscopic equations it can be shown that the wave-vector components of an SPP[2] wave are described as eqns. 2.4a ($\hat{x}$ direction in the metal-dielectric interface) and 2.4b ($\hat{z}$ direction in metal $j = 1$ and in the dielectric $j = 2$), where $\varepsilon_1(\omega)$ is the (frequency dependent) relative electric permittivity of metal, ε_2 is that of a dielectric, and $k_0 = \omega/c$.

$$k_x^2 = k_0^2 \frac{\varepsilon_1(\omega)\,\varepsilon_2}{\varepsilon_1(\omega) + \varepsilon_2} \qquad (2.4a) \qquad\qquad k_{j,z}^2 = k_0^2 \frac{\varepsilon_j^2}{\varepsilon_1(\omega) + \varepsilon_2} \qquad (2.4b)$$

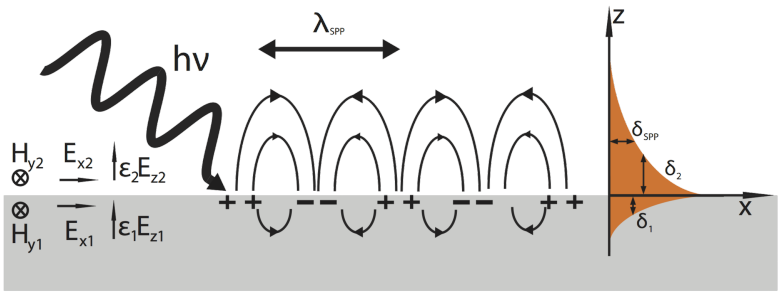

FIGURE 2.2: Sketch of a surface plasmon polariton wave propagating along a metallic surface. Wikimedia Commons, 2013

For metals, the real part of the relative permittivity is negative for certain frequencies. And, if a conductor *without* attenuation is considered, the conditions that provide a purely real k_x and a purely imaginary $k_{j,z}$ are [16]:

$$\varepsilon_1(\omega)\,.\,\varepsilon_2 < 0 \qquad (2.5a) \qquad\qquad \varepsilon_1(\omega) + \varepsilon_2 < 0 \qquad (2.5b)$$

2.2 Surface Plasmons

The conditions of eqn. set. 2.5 are fulfilled for frequencies lower than the characteristic surface plasmon frequency ω_{SP}. Even when considering a conductor with attenuation, regions that have imaginary components of the wave-vector appear below a certain frequency, i.e. surface plasmons will appear. The meaning and physical interpretation of these waves is discussed in this section.

[2]Surface plasmon polaritons (SPPs) are surface plasmons when produced in the interface between dielectric and metal [16].

Surface plasmons are "collective charge oscillations that occur at the interface between conductors and dielectrics" [37]. The unique properties of surface plasmons allow multiple applications. Including, but not limited to, single molecule detection, high resolution imaging at optical frequencies under the diffraction limit [37].

As it was mentioned in chapter 1, the history of plasmonics starts well before any scientific study of the optical properties of metallic nanostructures was made. However, it was not until almost half a century later, $1953 - 1956$, that David Pines described the energy losses related to electrons moving in the surface of a metal and coined the term *plasmon* [38–40], which refers to a quasiparticle resulting from the quantization of plasma oscillations [37].

The following year, 1957, sees the first theoretical description of *surface plasmons*, SPs. Rufus Richtie shows that near the surface of metals, plasmon modes can exist while studying energy losses for electrons in metallic thin films [37, 41]. By introducing a dielectric above the metallic surface, a new quasiparticle emerges - the *surface plasmon-polariton*, where the polariton is the quantum of polarization in the dielectric material. The SPP refers to both the charge motion in the metal (SP) as well as the electromagnetic wave in the dielectric (polariton) [34,42]. These SPP waves were, at the time, produced by impinging an electron beam into a metal surface. SPPs, or SPs for that matter, cannot be directly excited by light incident on the metallic surface [37, 43]. This is due to a "mismatch in wavelength of the SPP wave and the plane wave in the bulk dielectric partnering material prevents excitation of the SPP wave by direct coupling to a beam of light" [34].

Nevertheless, this constraint will be removed by 1968, when Andreas Otto and Erich Kretschmann with Heinz Raether developed methods for optically exciting plasmon resonances through the use of a prism with high refractive index near the metal vacuum interface - a surface plasmon is excited by an evanescent wave resulting from frustrated total reflection in the prism, as shown in fig. 2.3 [44–46]. This allowed experimentation on surface plasmons to become easily accessible to many scientists, and lead the field of SPs to shift perspectives from a fundamental study to an application driven research.

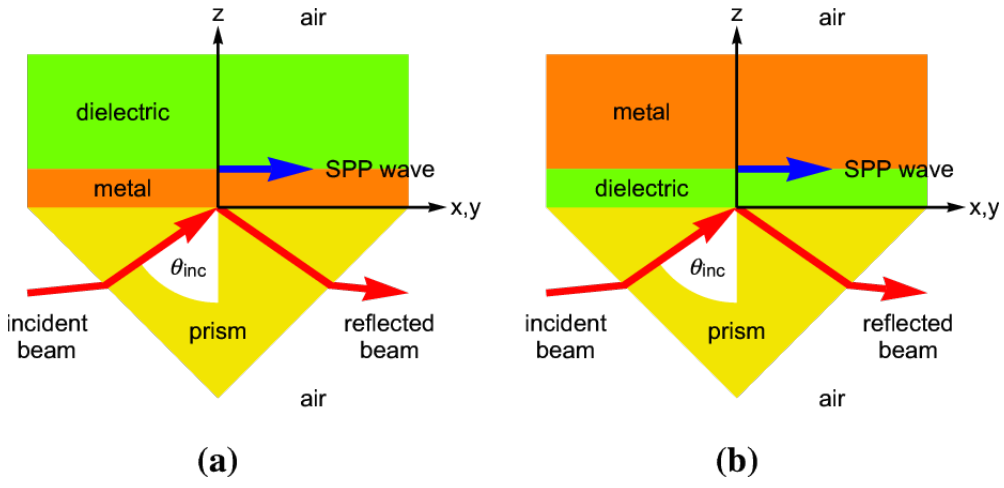

FIGURE 2.3: Scheme for exciting SPPs on a prism with the **(a)** Turbadar-Kretschmann-Raether and **(b)** Turbadar-Otto configurations [34].

A significant turning point for plasmonic related research was in 1998, when an extraordinary transmission of light due to light-plasmon coupling was observed through a sub-wavelength aperture in a thick metal film [47]. This arose interest in the use of plasmons for the fabrication

of waveguides as well as other photonic devices with sizes significantly smaller than the diffraction limit. This field of study became known as *plasmonics*, and it now encompasses all research related to surface plasmons in metallic films and plasmon resonances in metal nanoparticles (commonly referred to as *localized surface plasmons*) [43]. Shortly thereafter, Sir John Pendry proposes that a perfect lens can be achieved through negative refractive index materials, which can be obtained with plasmonic responses in a thin film of metal [48].

2.3 Localized Surface Plasmons

A few years later, a description for the optical properties of metallic nanoparticles in terms of surface plasmons is done by Uwe Kreibig and Peter Zacharias, where they compare the optical and electronic responses of gold and siver nanoparticles [49]. They were actually studying *localized surface plasmons* - the second fundamental excitation of plasmonics. LSPs, unlike surface plasmon polaritons, are "*non-propagating* excitations of the conduction electrons of metallic nanostructures coupled to an electromagnetic field" [16]. An effective restoring force on the conduction electrons, due to the curved nature of the nanoparticle, is responsible for the non-propagating resonance (propagation occurs in flat metallic-dielectric interfaces). This resonance is usually referred to as *localized surface plasmon resonance* (LSPR). LSPs can be directly excited by light unlike SPPs, that need to have a prism arrangement like the one shown in fig. 2.3 [16].

In order to study LSPs, the response of a metallic nanosphere (with frequency dependent relative electric permittivity $\varepsilon_m(\omega)$) interacting with an electromagnetic wave propagating in a dielectric medium (with ε_d) will be considered. This will lead to a resonance condition - apparent by the polarizability (α) of the particle.

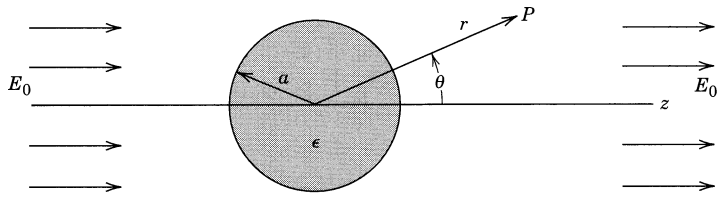

FIGURE 2.4: Metallic nanoparticle, $\varepsilon_m(\omega)$, in a host dielectric medium, ε_d, where a constant electric field is present [50].

The interaction between a metallic particle of size a with an electromagnetic field can be described through the *quasi-static approximation* as long as $a << \lambda$ (λ being the wavelength of the electromagnetic field). This particle is small enough, $a < 15\ [nm]$, to describe the problem through a constant electric field, $\boldsymbol{E_0} = E_0\hat{\boldsymbol{z}}$ [16].

From an electrostatic approach ($\boldsymbol{\nabla} \times \boldsymbol{E} = 0$), solutions for the Laplace equation, $\nabla^2\,\phi = 0$, appear in the form of the multipolar expansion of eqn. 2.6, where $P_\ell(\cos\theta)$ are the Legendre polynomials of ℓ^{th} order, and θ is the polar angle in spherical coordinates [50]. From these, an expression for the electric field can be obtained from $\boldsymbol{E} = -\boldsymbol{\nabla}\phi$.

$$\phi(r,\theta) = \sum_{\ell=0}^{\infty} \left[A_\ell\, r^\ell + \frac{B_\ell}{r^{\ell+1}} \right] P_\ell(\cos\theta) \tag{2.6}$$

Since the electric potential must be finite, and reconnect with E_0's potential when r approaches infinity, eqn. 2.7a is obtained. The electric potential also has to be finite in the center of the sphere, i.e. $r = 0$, so eqn. 2.7b is written.

$$\phi_{in}(r,\theta) = \sum_{\ell=0}^{\infty} \tilde{p}_{\ell}^{(in)}\, r^{\ell}\, P_{\ell}(\cos\theta) \tag{2.7a}$$

$$\phi_{out}(r,\theta) = \sum_{\ell=0}^{\infty} \left[\frac{p_{\ell}^{(out)}}{r^{\ell+1}} - r\, E_0 \delta_{\ell,1} \right] P_{\ell}(\cos\theta) \tag{2.7b}$$

Continuity in the normal and tangential components of the displacement field and electric field, respectively, in the surface where metal and dielectric meet ($r = a$) provide eqn. set 2.8.

$$-\varepsilon_m(\omega) \left.\frac{\partial \phi_{in}}{\partial r}\right|_{r=a} = -\varepsilon_d \left.\frac{\partial \phi_{out}}{\partial r}\right|_{r=a} \tag{2.8a}$$

$$-\frac{1}{a} \left.\frac{\partial \phi_{in}}{\partial \theta}\right|_{r=a} = -\frac{1}{a} \left.\frac{\partial \phi_{out}}{\partial \theta}\right|_{r=a} \tag{2.8b}$$

When the expressions of the electric potentials, eqn. set 2.7, are substituted into these boundary conditions of eqn. set 2.8, the following expressions are obtained (and can be traced back to [50,51]).

$$\phi_{in}(r,\theta) = -\frac{3\,\varepsilon_d}{\varepsilon_m(\omega) + 2\varepsilon_d} E_0\, r\, \cos\theta \tag{2.9a}$$

$$\phi_{out}(r,\theta) = -E_0\, r\, \cos\theta + \frac{\varepsilon_m(\omega) - \varepsilon_d}{\varepsilon_m(\omega) + 2\varepsilon_d} E_0\, a^3\, \frac{\cos\theta}{r^2} \tag{2.9b}$$

The physical interpretation of eqn. 2.9b is a superposition of two electric potentials - the external potential ($-E_0\, r \cos\theta$) and the potential of an electric dipole. To put this in perspective, the equation of a dipole (situated in $r = 0$) in a dielectric medium of relative electric permittivity ε_d is defined as eqn. 2.10, where $\boldsymbol{p}$ is the dipole moment [51].

$$\phi_{dip} = \frac{\boldsymbol{p} \cdot \hat{\boldsymbol{r}}}{4\pi\varepsilon_0\varepsilon_d\, r^2} = \frac{p\, \cos\theta}{4\pi\varepsilon_0\varepsilon_d\, r^2} \tag{2.10}$$

This observation results in an expression of ϕ_{out} in terms of the dipole moment p of the nanoparticle, eqn. 2.11. And of a corresponding expression for the dipole moment, eqn. 2.12.

$$\phi_{out} = -E_0\, r\, \cos\theta + \frac{\boldsymbol{p} \cdot \hat{\boldsymbol{r}}}{4\pi\varepsilon_0\varepsilon_d\, r^2} \tag{2.11}$$

$$\boldsymbol{p} = 4\pi\varepsilon_0\varepsilon_d\, a^3\, \frac{\varepsilon_m(\omega) - \varepsilon_d}{\varepsilon_m(\omega) + 2\varepsilon_d} \boldsymbol{E_0} \tag{2.12}$$

With the polarizability of the particle as α, described as $\boldsymbol{p} = \alpha\, \boldsymbol{E_0}$, then eqn. 2.13 defines it, and it shows the same form of the Clausius-Mossotti relation [50].

$$\alpha(\omega) = 4\pi\varepsilon_0\, a^3\, \varepsilon_d\, \frac{\varepsilon_m(\omega) - \varepsilon_d}{\varepsilon_m(\omega) + 2\varepsilon_d} \tag{2.13}$$

This is the central result of this derivation, and it is an important one since the polarizability can provide coefficients related to scattering, absorption, extinction, heating, etc [52]. It should be noted that α depends on the radius of the particle, which must be smaller than $100\ [nm]$ due to the quasi-static approximation. For larger particles, the polarizability must be obtained through Mie theory [53]. This is a complex and frequency dependent polarizability because the relative electric permittivity of the metal depends on the frequency of the incident electromagnetic wave, eqn. 2.14 (Drude model).

$$\varepsilon_m(\omega) = 1 - \frac{\omega_p^2}{\omega(\omega + i\,\gamma)} = \varepsilon'_m + i\,\varepsilon''_m \tag{2.14}$$

Figure 2.5 shows the complex polarizability of silver as a function of the frequency, $E = \hbar\omega$, of the incident EM wave [16].

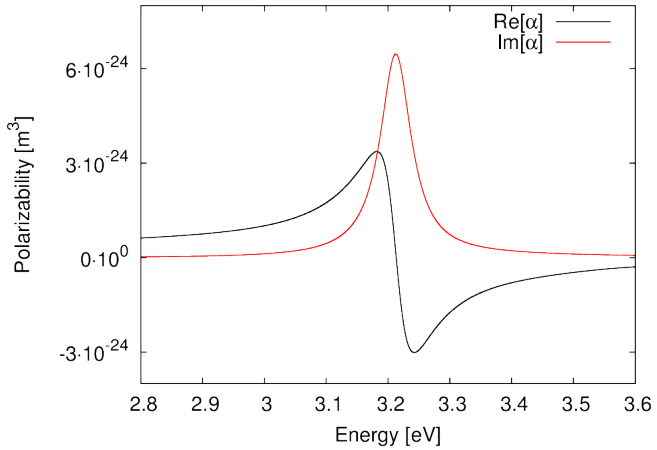

FIGURE 2.5: Polarizability of a silver nanoparticle vs. EM wave energy.

However, when considering a conductor without attenuation (or in the high-frequency domain), i.e. $\gamma << \omega$ in eqn. 2.14 (where ω_p is the plasmon frequency), the metal permittivity is predominantly real. From this it follows that a singularity for the polarizability exists when $\varepsilon_m(\omega_0) = -2\varepsilon_d$ (Fröhlich condition).

There is a problem here. Real metals have non-negligible damping, and thus display losses. These losses are related to the positive, imaginary component of the relative electric permittivity of the metal (ε''_m). This positive ε''_m is the only responsible of the positive imaginary part of the polarizability of fig. 2.5. It follows from this that a $\Im[\alpha] > 0$ has a physical representation of dispersion of energy within the medium. This means that in order to obtain the same behaviour of LSP resonance, but without the losses, some loss compensation must be done. The most promising method to achieve this is to couple the particle with "active compounds which are able to transfer energy from a pump and therefore amplify the desired response" [54].

Similar studies can be made for other types of nanoparticles, since different geometries have unique properties. Out of these different geometries, we choose to describe a metallic nanoshell because, how it will be thoroughly explained later, this design provides interesting physical properties and it is easier both to synthesize and to model.

2.4 Loss-Compensation

In order to fight the losses related to the imaginary component of the electric permittivity of the metal, the use of optical gain material is commonly used [17, 55–59]. Examples of optical gain material are polymers with dye, quantum dots, fluorescent molecules, or rare-earth ions [52, 56, 60–62]. Gain materials are commonly used in lasers in order to obtain optical gain, which results from a transition from a high energy state to a low energy state. This is achieved by obtaining a majority of quantum elements in the higher energy state than in the lower energy state, i.e. a population inversion.

If losses in a material are related to a positive, imaginary component of the electric permittivity, then the opposite of this can be interpreted as gain in a material. That is, if a certain material has $\Im[\varepsilon] < 0$, one can say that it is a gain material [63]. For this work, a gain material with a frequency dependent permittivity, $\varepsilon_g(\omega)$, will be considered. In the steady state, the gain medium can be defined with a "single Lorentzian emission line shape" [54] centered at the gain frequency (ω_g), and in the steady state can be described as eqn. 2.15.

$$\varepsilon_g(\omega) = -\frac{\varepsilon_g''(\omega_g)\,\Delta}{2(\omega-\omega_g)+i\Delta} \tag{2.15}$$

This equation for the permittivity of the gain material is added to that of a linear dielectric and the host permittivity is obtained: $\varepsilon_h(\omega) = \varepsilon_d + \varepsilon_g(\omega)$. This leads to a frequency dependent host permittivity ($\varepsilon_h(\omega) = \varepsilon_h'(\omega) + i\varepsilon_h''(\omega)$), that for the case of $\varepsilon_g''(\omega_g) = -2.33$ is represented by fig. 2.6.

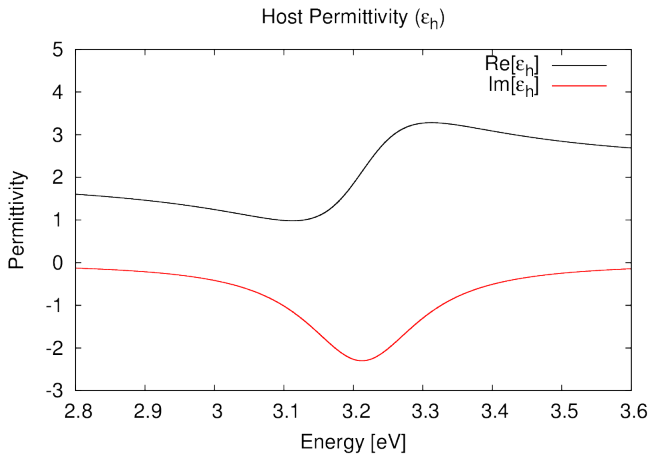

FIGURE 2.6: Permittivity of host medium (linear dielectric and optical gain material).

The negative imaginary permittivity in fig. 2.6 is exactly what is needed to compensate for losses in the metal. Part of the aim of this work is to figure out the value of $\varepsilon_g''(\omega_g)$ that would allow for a high-intensity LSP in a nanoshell geometry.

2.5 Surface Plasmon Amplification by Stimulated Emission of Radiation (SPASER)

Through a quantization of the surface plasmon fields and their stimulated emission, the existence of "temporally coherent high-intensity fields of selected surface plasmon modes that can be strongly localized on the nanoscale" were demonstrated by Bergman and Stockman in their seminal paper that introduced the spaser [26]. However, since noble metals experience strong losses when optical frequency fields are impinged upon them, gain material is used to mitigate this. Stockman describes the gain through the optical-Bloch formalism (Appendix A) and copules them to a second-quantization of the plasmonic field in a box. This results in a hamiltonian with ladder operators relating to the creation and destruction of surface plasmon modes, a term related to the energy of the gain medium, and a term for the coupling of the electric field with the dipolar moment of each gain element (eqn. 2.16).

$$H = \hbar \sum_n \omega_n a_n^\dagger a_n + H_g - \sum_p \boldsymbol{E}(\boldsymbol{r}_d) \cdot \boldsymbol{d}^{(p)} \tag{2.16}$$

In the following chapter a thorough description of the nanoshell geometry will be made. This will include the classical model to obtain the steady state polarizability, time-dynamical equations for the materials and the fields, numerical linear and non-linear solutions for these equations, and an eigenvalues description for them. The metal is considered to follow a Drude-Sommerfeld model, which provides a description of the polarization and electric field inside the metal. The gain material will be approximated as an atomic two-level system with optical-Bloch equations (see Appendix A).

Chapter 3

Theory

3.1 Doped Metallic Nanoshell

Here is where we really start. A theoretical/numerical study of a silver nanoshell with externally pumped optical gain material on its core excited by an external electric field is done. The geometry that is being considered is portrayed by fig. 3.1. This nanoshell has an inner radius a_1 and outer radius a_2.

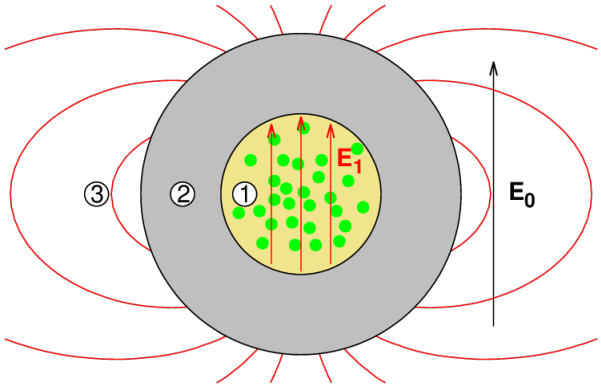

FIGURE 3.1: Nanoshell geometry.

Region 1 is a sphere of radius a_1, and it has two components that create its permittivity ε_1. The first component is a background dielectric that is constant in the frequency region of interest, ε_b. Then, optical gain material is added. The permittivity that the gain contributes is dependent on the frequency of the external field, $\boldsymbol{E}_0$, and has real and imaginary components, $\varepsilon_g(\omega)$.

Region 2 represents a metal shell of inner radius a_1 and outer radius a_2, that has complex frequency dependent permittivity, $\varepsilon_2(\omega)$. We define the relation between the radii as $\rho = a_1/a_2$.

Finally, region 3 is the linear dielectric of constant electric permittivity ε_3 of the solvent used, and it can be ethanol, water, silica, etc.

3.1.1 Gain Material

The gain material is described with a two-level system and the optical-Bloch formalism (described in Appendix A). Two equations are retrieved from this - one that describes the time dynamical population inversion of the system, 3.1a, and one that describes the time dependent

coherence of the gain molecules between excited $|2\rangle$ and ground $|1\rangle$ states, ρ_{12}, 3.1b. This coherence is related to the dipole moment of the gain molecules ($\boldsymbol{\mu}$) which in turn is related to the density of dipole moments of the gain material, $\boldsymbol{P}_{1,g}$

$$\frac{d\,\rho_{12}}{d\,t} - \left(i\omega_{21} - \frac{1}{\tau_2}\right)\rho_{12} = -\frac{i\,H_{12}N}{\hbar} = \frac{iN\,\boldsymbol{\mu}\cdot\boldsymbol{E_1}}{\hbar} \tag{3.1a}$$

$$\frac{d\,N}{d\,t} + \frac{N-N_0}{\tau_1} = \frac{2i(\rho_{12}-\rho_{21})\,\boldsymbol{\mu}\cdot\boldsymbol{E_1}}{\hbar} \tag{3.1b}$$

By defining a tensor that accounts for the dipole moment of the gain molecules as was done in eqn. A.15, the polarization density of the gain elements can be defined as $\boldsymbol{P}_{1,g} = n_g\langle\widehat{\mu}\rangle$, where n_g is the density of gain molecules. The average over the dipole moments of the molecules is done in the following way: (i) the density matrix is used to average for the quantum states of the system and (ii) a solid angle integration averages over the direction of all the gain molecules, which are randomly oriented to begin with. This provides a relation between ρ_{12} and the macroscopic density of dipole moments of gain, given by eqn. 3.2, where Ω is the solid angle.

$$\boldsymbol{P}_{1,g} = \frac{n_g}{4\pi}\int_0^{4\pi}(\rho_{12}+\rho_{21})\boldsymbol{\mu}d\Omega \tag{3.2}$$

Now, defining the field $\boldsymbol{\Pi} = \dfrac{n_g}{4\pi}\displaystyle\int_\Omega \rho_{12}\boldsymbol{\mu}d\Omega$, and knowing that the density matrix is hermitian, $\rho_{mn} = \rho^*_{nm}$, eqn. 3.2 can be rewritten.

$$\boldsymbol{P}_{1,g} = \frac{n_g}{4\pi}\int_0^{4\pi}(\rho_{12}+\rho^*_{12})\boldsymbol{\mu}d\Omega = \boldsymbol{\Pi}+\boldsymbol{\Pi}^* \tag{3.3}$$

Taking into account the background dielectric, which has electric susceptibility χ_b, the polarization of region 1 is defined by eqn. 3.4.

$$\boldsymbol{P}_1 = \varepsilon_0\chi_b\boldsymbol{E}_1 + \boldsymbol{\Pi} + \boldsymbol{\Pi}^* \tag{3.4}$$

This means that eqn. set 3.1 can be recast into the following equations, using the field $\boldsymbol{\Pi}$, and knowing that $\displaystyle\int_0^{4\pi}(\boldsymbol{\mu}\cdot\boldsymbol{E_1})\boldsymbol{\mu}d\Omega = \frac{4\pi}{3}\mu^2\boldsymbol{E_1}$:

$$\frac{d\,\boldsymbol{\Pi}}{d\,t} - \left(i\omega_{21} - \frac{1}{\tau_2}\right)\boldsymbol{\Pi} = \frac{in_gN\mu^2}{3\hbar}\boldsymbol{E_1} \tag{3.5a}$$

$$\frac{d\,N}{d\,t} + \frac{N-N_0}{\tau_1} = \frac{2i}{n\hbar}(\boldsymbol{\Pi}-\boldsymbol{\Pi}^*)\cdot\boldsymbol{E_1} \tag{3.5b}$$

Now, the *rotating wave approximation* (eqn. set 3.6) is used to simplify the system. Assuming that the frequency of the probe electric field $\boldsymbol{E}_0$ is near resonant ($\omega \sim \omega_{21}$) and considering a harmonic form for all time dependent variables, $e^{-i\omega t}$, the equations for the time envelopes of $\tilde{\boldsymbol{\Pi}}$, $\tilde{\boldsymbol{E_1}}$, and $\tilde{\boldsymbol{P_1}}$ [64]:

$$\boldsymbol{\Pi} = \tilde{\boldsymbol{\Pi}}(t)\, e^{i\omega t} \tag{3.6a}$$

$$\boldsymbol{E_1} = \frac{1}{2}\left[\tilde{\boldsymbol{E_1}}(t)\, e^{-i\omega t} + \tilde{\boldsymbol{E_1^*}}(t) e^{i\omega t}\right] \tag{3.6b}$$

$$\boldsymbol{P_1} = \frac{1}{2}\left[\tilde{\boldsymbol{P_1}}(t)\, e^{-i\omega t} + \tilde{\boldsymbol{P_1^*}}(t) e^{i\omega t}\right] \tag{3.6c}$$

Inserting this into eqn. 3.4 and eqn. set 3.5 results in:

$$\frac{d\,\boldsymbol{\Pi}}{d\,t} + \left[i(\omega - \omega_{21}) + \frac{1}{\tau_2}\right]\boldsymbol{\Pi} = \frac{inN\mu^2}{6\hbar}\boldsymbol{E_1^*} \tag{3.7a}$$

$$\frac{d\,N}{d\,t} + \frac{N - N_0}{\tau_1} = \frac{i}{n\hbar}(\boldsymbol{E_1}\cdot\boldsymbol{\Pi} - \boldsymbol{E_1^*}\cdot\boldsymbol{\Pi^*}) \tag{3.7b}$$

$$\boldsymbol{P_1} = \varepsilon_0\chi_b\boldsymbol{E_1} + 2\boldsymbol{\Pi^*} \tag{3.7c}$$

From now on, tildes will be omitted and all fields will be assumed to be represented by their time envelope, which are the physically relevant quantities.

3.1.2 Metal

The electric field $\boldsymbol{E_2}$ acts on the electrons in the metal. This interaction can be described using the free electron model, eqn. 3.8.

$$\frac{d^2\boldsymbol{r}}{dt^2} + 2\gamma\frac{d\boldsymbol{r}}{dt} = \frac{e}{m_e}\boldsymbol{E_2} \tag{3.8}$$

Where $\boldsymbol{r}$ is the displacement of the electron from it's equilibrium position, e is the elementary charge, m_e is the electron's mass, and γ is a collision frequency [65]. If n_e is the density of electrons in the metal, then the polarization density is defined as $\boldsymbol{P_2} = n_e\, e\, \boldsymbol{r}$. This means that the time evolution of $\boldsymbol{P_2}$ can be written as eqn. 3.9, by defining the plasma frequency as $\omega_p^2 = \dfrac{n_e\, e^2}{m_e\varepsilon_0}$.

$$\frac{d^2\,\boldsymbol{P_2}}{dt^2} + 2\gamma\frac{d\boldsymbol{P_2}}{dt} = \varepsilon_0\,\omega_p\,\boldsymbol{E_2} \tag{3.9}$$

Considering the rotating wave approximation one more time, but this time with eqn. set 3.10, will simplify eqn. 3.9.

$$\boldsymbol{E_2} = \frac{1}{2}\left[\tilde{\boldsymbol{E_2}}(t)e^{-i\omega t} + \tilde{\boldsymbol{E_2^*}}(t)e^{i\omega t}\right] \tag{3.10a}$$

$$\boldsymbol{P_2} = \frac{1}{2}\left[\tilde{\boldsymbol{P_2}}(t)e^{-i\omega t} + \tilde{\boldsymbol{P_2^*}}(t)e^{i\omega t}\right] \tag{3.10b}$$

Applying these considerations, aking the second time derivative of the slowly varying polarization densities ($\tilde{\boldsymbol{P_2}}(t)$ and $\tilde{\boldsymbol{P_2^*}}(t)$) to be negligible, and omitting the tildes once more, eqn. 3.9 transforms to:

$$\frac{d\boldsymbol{P_2}}{dt} - \frac{\omega^2 + 2i\gamma\omega}{2(\gamma - i\omega)}\boldsymbol{P_2} = \frac{\varepsilon_0\,\omega_p^2}{2(\gamma - i\omega)}\boldsymbol{E_2} \tag{3.11}$$

From this equation it is possible to determine the steady state permittivity of the metal $\varepsilon_m(\omega)$ using the relation $\boldsymbol{P}_2 = \varepsilon_0(\varepsilon_m - 1)\boldsymbol{E_2}$ and $d\boldsymbol{P_2}/dt = 0$. This results in eqn. 3.12, which is the classical Drude model [52, 66].

$$\varepsilon_m(\omega) = 1 - \frac{\omega_p^2}{\omega(\omega + i\gamma)} \tag{3.12}$$

3.2 Nanoshell and Gain Polarizability

A classical formulation of the polarizability is presented in Appendix B. This calculation is only valid for the nanoshell with no active molecules in region 1. In order to account for these, the fields that where obtained in the previous sections will be considered.

Now that gain material has been added to the system, it is not possible to say that $\boldsymbol{\nabla} \cdot \boldsymbol{E} = 0$. Instead, and assuming there are no free charges, the divergence of the displacement field, $\boldsymbol{D} = \varepsilon_0 \boldsymbol{E} + \boldsymbol{P}$, where $\boldsymbol{P}$ is the polarization, ought to be zero.

Since the size of the nanoshell is small enough to consider the quasi-static approximation, we can say that the electric field is irrotational, i.e. $\boldsymbol{E} = -\boldsymbol{\nabla}\phi$. From here, the rotational of $\boldsymbol{D}$ can be expressed as: $\boldsymbol{\nabla} \times \boldsymbol{D} = \boldsymbol{\nabla} \times \boldsymbol{P}$. This means if $\boldsymbol{P}$ is irrotational, then the displacement field is also irrotational, which leads to $\boldsymbol{D} = -\boldsymbol{\nabla}\xi$. Additionally, and considering no free charges, the divergence of $\boldsymbol{D}$ is zero. Consequently, the field related to $\boldsymbol{D}$ follows Laplace's equation, $\nabla^2\xi = 0$. Since the polarization is considered to be irrotational, then it is possible to write: $\boldsymbol{\Pi} = -\boldsymbol{\nabla}\psi_1$ and $\boldsymbol{P_2} = -\boldsymbol{\nabla}\psi_2$. This leads to the following expressions for the displacement field in all three regions (eqn. set 3.13).

$$\boldsymbol{D_1} = \varepsilon_0 \boldsymbol{E_1} + \varepsilon_0 \chi_b \boldsymbol{E_1} + 2\boldsymbol{\Pi^*} = \varepsilon_0 \varepsilon_b \boldsymbol{E_1} + 2\boldsymbol{\Pi^*} = \varepsilon_0 \varepsilon_b \left(-\boldsymbol{\nabla}\phi_1\right) + 2\left(-\boldsymbol{\nabla}\psi_1\right)^* \tag{3.13a}$$

$$\boldsymbol{D_2} = \varepsilon_0 \boldsymbol{E_2} + \varepsilon_0 \chi_m \boldsymbol{P_2} = \varepsilon_0 \left(-\boldsymbol{\nabla}\phi_2\right) + \varepsilon_0 \chi_m \left(-\boldsymbol{\nabla}\psi_2\right) \tag{3.13b}$$

$$\boldsymbol{D_3} = \varepsilon_0 \varepsilon_3 \boldsymbol{E_3} = \varepsilon_0 \varepsilon_3 \left(-\boldsymbol{\nabla}\phi_3\right) \tag{3.13c}$$

From the fact that in all these regions there are no free charges and thus the divergence of the displacement field is zero, it is clear that one solution for these equations is Laplace's equation for $\phi_{1,2,3}$ and for $\psi_{1,2}$. This means that the solutions for the polarization potentials in a system with azimuthal symmetry can be expressed as eqn. 3.14.

$$\psi_{1,2}(r, \theta, t) = \sum_{\ell=0}^{\infty} \left[q_\ell^{(1,2)} + \frac{\sigma_\ell^{(1,2)}}{r^{\ell+1}} \right] P_\ell(\cos\theta) \tag{3.14}$$

Additionally, the electric potentials can be expressed as it was done in Appendix A (eqn. set 3.15), where as the gain is in a uniform electric field, $\ell = 1$ is the only allowed mode - even in the non-linear regime.

$$\phi_1(r,\theta,t) = \left[\frac{p^{(2)}}{\rho^3 a_2^3} + \frac{p^{(3)}-p^{(2)}}{a_2^3} - E_0\right] r\,\cos\theta \tag{3.15a}$$

$$\phi_2(r,\theta,t) = \left[\frac{p^{(3)}-p^{(2)}}{a_2^3} - E_0\right] r\,\cos\theta + p^{(2)}\frac{\cos\theta}{r^2} \tag{3.15b}$$

$$\phi_3(r,\theta,t) = -E_0\, r\,\cos\theta + p^{(3)}\frac{\cos\theta}{r^2} \tag{3.15c}$$

Applying regularity conditions for eqns. 3.14 when $r = 0$, and setting $\sigma_1^{(2)} = \sigma$, the following equations are obtained:

$$\psi_1 = q^{(1)}\, r\cos\theta$$
$$\psi_2 = q^{(2)}\, r + \frac{\sigma}{r^2}\cos\theta$$

Determining the radial derivatives of these potentials, and the tangential derivatives of ϕ_1 and ψ_1 gives:

$$E_1^r = \left[E_0 - \frac{p^{(2)}}{\rho^3 a_2^3} - \frac{p^{(3)}-p^{(2)}}{a_2^3}\right]\cos\theta \tag{3.16a}$$

$$E_2^r = \left[E_0 - \frac{p^{(3)}-p^{(2)}}{a_2^3}\right]\cos\theta + 2p^{(2)}\frac{\cos\theta}{r^3} \tag{3.16b}$$

$$E_3^r = E_0\cos\theta + 2p^{(3)}\frac{\cos\theta}{r^3} \tag{3.16c}$$

$$\Pi^r = -q^{(1)}\cos\theta \tag{3.16d}$$

$$P_2^r = -q^{(2)}\cos\theta + 2\sigma\frac{\cos\theta}{r^3} \tag{3.16e}$$

$$E_1^\theta = -\left[E_0 - \frac{p^{(2)}}{\rho^3 a_2^3} - \frac{p^{(3)}-p^{(2)}}{a_2^3}\right]\sin\theta \tag{3.16f}$$

$$\Pi^\theta = q^{(1)}\sin\theta \tag{3.16g}$$

From here, $\boldsymbol{E_1}\cdot\boldsymbol{\Pi} - \boldsymbol{E_1}\cdot\boldsymbol{\Pi}^* = -2\Im[\boldsymbol{E_1}\cdot\boldsymbol{\Pi}]$ is necessary to recast eqn. 3.7b. In terms of the multipolar expansion it can be defined as:

$$-2\Im[\boldsymbol{E_1}\cdot\boldsymbol{\Pi}] = 2q^{(1)}\left[E_0 - \frac{p^{(2)}}{\rho^3 a_2^3} - \frac{p^{(3)}-p^{(2)}}{a_2^3}\right]$$

Substituting this equation and eqns. 3.16a- 3.16e into eqns. 3.7a and 3.11, the following four equations are obtained.

$$\frac{dq^{(1)}}{dt} + \left[i(\omega - \omega_{21}) + \frac{1}{\tau_2}\right] q^{(1)} = -\frac{inN\mu^2}{6\hbar}\left[E_0^* - \frac{p^{(2)*}}{\rho^3 a_2^3} - \frac{p^{(3)*} - p^{(2)*}}{\rho^3 a_2^3}\right] \tag{3.17a}$$

$$\frac{dN}{dt} + \frac{N - N_0}{\tau_1} = \frac{2}{n\hbar}\Im\left\{q^{(1)}\left[E_0 - \frac{p^{(2)}}{\rho^3 a_2^3} - \frac{p^{(3)} - p^{(2)}}{a_2^3}\right]\right\} \tag{3.17b}$$

$$\frac{dq^{(2)}}{dt} - \frac{\omega^2 + 2i\gamma\omega}{2(\gamma - i\omega)} q^{(2)} = -\frac{\varepsilon_0\omega_p^2}{2(\gamma - i\omega)}\left[E_0 - \frac{p^{(3)} - p^{(2)}}{a_2^3}\right] \tag{3.17c}$$

$$\frac{d\sigma}{dt} - \frac{\omega^2 + 2i\gamma\omega}{2(\gamma - i\omega)}\sigma = \frac{\varepsilon_0\omega_p^2}{2(\gamma - i\omega)} p^{(2)} \tag{3.17d}$$

3.2.1 Boundary Conditions

The boundary conditions on the radial components of the electric and polarization fields in $a_1 = \rho a_2$ and in a_2 are:

$$\begin{aligned}
[\varepsilon_0\varepsilon_b E_1^r + 2\Pi^{r*}]_{r=\rho a_2} &= [\varepsilon_0 E_2^r + P_2^r]_{r=\rho a_2} \\
[E_2^r + P_2^r]_{r=a_2} &= \varepsilon_3 E_3^r|_{r=a_2}
\end{aligned}$$

These boundary conditions and the equations that describe the electric and polarization density fields (eqn. set 3.17) result in equations for $p^{(2,3)}$:

$$\begin{aligned}
p^{(2)} = &-\frac{\rho^3(\varepsilon_b - 1)}{\varepsilon_b + 2 - \rho^3(\varepsilon_b - 1)} p^{(3)} + \rho^3 a_2^3 \frac{(\varepsilon_b - 1)}{\varepsilon_b + 2 - \rho^3(\varepsilon_b - 1)} E_0 + \\
&+ \frac{\rho^2 a_2^3}{\varepsilon_0}\left(\frac{q^{(2)} - 2q^{(1)*} - \dfrac{2\sigma}{\rho^3 a_2^3}}{\varepsilon_b + 2 - \rho^3(\varepsilon_b - 1)}\right)
\end{aligned}$$

$$\begin{aligned}
p^{(3)} = &\, a_2^3 \frac{(1 - \varepsilon_3)(\varepsilon_b + 2) + \rho^3(\varepsilon_b - 1)(\varepsilon_3 + 2)}{(\varepsilon_b + 2)(1 + 2\varepsilon_3) + 2\rho^2(\varepsilon_b - 1)(1 - \varepsilon_3)} E_0 + \\
&- \frac{a_2^3}{\varepsilon_0} \frac{6\rho^3 q^{(1)*} + (1 - \rho^3)\left[(\varepsilon_b + 2)q^{(2)} - (\varepsilon_b - 1)\frac{2\sigma}{a_2^3}\right]}{(\varepsilon_b + 2)(1 + 2\varepsilon_3) + 2\rho^2(\varepsilon_b - 1)(1 - \varepsilon_3)}
\end{aligned}$$

3.3 Time Dynamical System of Equations

At this point, the metal's electric permittivity (eqn. 3.12) along with the linear gain permittivity (obtained in Appendix A) are used to simplify eqn. set 3.17 as described below.

$$\varepsilon_h''(\omega_{21}) = -\frac{n\mu^2\tau_2}{3\hbar\varepsilon_0} \tag{3.18}$$

$$\frac{dq^{(1)}}{dt} + \left[i(\omega - \omega_{21}) + \frac{1}{\tau_2}\right] q^{(1)} = \frac{iN\varepsilon_0\varepsilon_h''(\omega_{21})}{2\tau_2}\left[E_0^* - \frac{p^{(2)*}}{\rho^3 a_2^3} - \frac{p^{(3)*} - p^{(2)*}}{\rho^3 a_2^3}\right] \tag{3.19a}$$

$$\frac{dN}{dt} + \frac{N - N_0}{\tau_1} = \frac{2}{n\hbar}\Im\left\{q^{(1)}\left[E_0 - \frac{p^{(2)}}{\rho^3 a_2^3} - \frac{p^{(3)} - p^{(2)}}{a_2^3}\right]\right\} \tag{3.19b}$$

$$\frac{dq^{(2)}}{dt} - \frac{i\omega\omega_p^2}{\omega^2(1-\varepsilon_m) + \omega_p^2} q^{(2)} = -\varepsilon_0 \frac{i\omega\omega_p^2(1-\varepsilon_m)}{\omega^2(1-\varepsilon_m) + \omega_p^2}\left[E_0 - \frac{p^{(3)} - p^{(2)}}{a_2^3}\right] \tag{3.19c}$$

$$\frac{d\sigma}{dt} - \frac{i\omega\omega_p^2}{\omega^2(1-\varepsilon_m) + \omega_p^2}\sigma = -\varepsilon_0 \frac{i\omega\omega_p^2(1-\varepsilon_m)}{\omega^2(1-\varepsilon_m) + \omega_p^2} p^{(2)} \tag{3.19d}$$

For the numerical solutions all quantities are made to be dimensionless. To do so, the following variable changes are made: $\sigma \to \frac{\sigma}{\varepsilon_0\rho^3 a_2^3}$, $t \to \omega_p t$, and $\omega \to \omega/\omega_p$. Additionally, defining $p_2 = \frac{p^{(2)}}{\rho^3 a_2^3}$, $p_3 = \frac{p^{(3)}}{a_2^3}$, $q_1 = \frac{q^{(1)}}{\varepsilon_0}$, and $q_2 = \frac{q^{(2)}}{\varepsilon_0}$ lead to:

$$\frac{dq_1}{dt} + \left[i(\omega - \omega_{21}) + \frac{1}{\tau_2}\right] q_1 = \frac{iN\varepsilon_h''(\omega_{21})}{2\tau_2 N_0}\left[E_0^* - p_3^* - (1-\rho^3)p_2^*\right] \tag{3.20a}$$

$$\frac{dq_2}{dt} - \frac{i\omega}{\omega^2(1-\varepsilon_m) + 1} q_2 = -\frac{i\omega(1-\varepsilon_m)}{\omega^2(1-\varepsilon_m) + 1}\left[E_0 - p_3 + \rho^2 p_2\right] \tag{3.20b}$$

$$\frac{d\sigma}{dt} - \frac{i\omega}{\omega^2(1-\varepsilon_m) + 1}\sigma = -\frac{i\omega(1-\varepsilon_m)}{\omega^2(1-\varepsilon_m) + 1} p^{(2)} \tag{3.20c}$$

3.3.1 Recovering the Classical Polarizability

If the linear ($N = N_0$) case is considered, eqn. 3.19b becomes irrelevant, since the population inversion would have no time dependency. Moreover, taking steady state solutions for eqn. set 3.19 would lead to:

$$\left[i(\omega - \omega_{21}) + \frac{1}{\tau_2}\right] q^{(1)} = \frac{i\varepsilon_0\varepsilon_h''(\omega_{21})N_0}{2\tau_2}\left[E_0^* - \frac{p_{ss}^{(2)*}}{\rho^3 a_2^3} - \frac{p_{ss}^{(3)*} - p_{ss}^{(2)*}}{\rho^3 a_2^3}\right] \tag{3.21a}$$

$$\frac{i\omega\omega_p^2}{\omega^2(1-\varepsilon_m) + \omega_p^2} q^{(2)} = \varepsilon_0 \frac{i\omega\omega_p^2(1-\varepsilon_m)}{\omega^2(1-\varepsilon_m) + \omega_p^2}\left[E_0 - \frac{p_{ss}^{(3)} - p_{ss}^{(2)}}{a_2^3}\right] \tag{3.21b}$$

$$\frac{i\omega\omega_p^2}{\omega^2(1-\varepsilon_m) + \omega_p^2}\sigma = \varepsilon_0 \frac{i\omega\omega_p^2(1-\varepsilon_m)}{\omega^2(1-\varepsilon_m) + \omega_p^2} p_{ss}^{(2)} \tag{3.21c}$$

After lengthy calculations, one can solve these equations for $p_{ss}^{(3)}$ and $p_{ss}^{(2)}$. The model would appear to be correct since the resulting expressions for these terms are exactly the ones obtained for the classical case (Appendix B), with the steady state definition for the gain permittivity:

$$\varepsilon_h = \varepsilon_b - \frac{\varepsilon_h''(\omega_{21})N\Delta}{2(\omega - \omega_{21}) + i\Delta}$$

After assigning this value to the host permittivity, eqn. set 3.22 describe the values of $p_{ss}^{(3)}$ and $p_{ss}^{(2)}$. These values match exactly with those of eqns. B.18 and B.19, respectively, since $\varepsilon_h \to \varepsilon_1$ and $\varepsilon_m \to \varepsilon_2$.

$$p_{ss}^{(3)} = a_2^3 \frac{(\varepsilon_m - \varepsilon_3)(\varepsilon_h + 2\varepsilon_m) + \rho^3(\varepsilon_h - \varepsilon_m)(\varepsilon_3 + 2\varepsilon_m)}{(\varepsilon_m + 2\varepsilon_3)(\varepsilon_h + 2\varepsilon_m) + 2\rho^3(\varepsilon_m - \varepsilon_3)(\varepsilon_h - \varepsilon_m)} E_0 \tag{3.22a}$$

$$p_{ss}^{(2)} = \frac{\rho^3 a_2^3(\varepsilon_h - \varepsilon_m)E_0 - \rho^3(\varepsilon_h - \varepsilon_m)p^{(3)}}{(\varepsilon_h + 2\varepsilon_m) - \rho^3(\varepsilon_h - \varepsilon_m)} \tag{3.22b}$$

Chapter 4

Results

In order to achieve a thorough understanding of the nanoshell system, the equations that define its temporal evolution (eqn. set 4.1) will be studied with a series of numerical tools. The first test that was made was checking if the steady state solutions ($d/dt = 0$) for $p_{2,3}$ result in the formula for the classical nanoshell that was obtained in Appendix B. As it was mentioned in 3.3.1, this was analytically obtained. If the system is not dominated by the response of the quantum emitters, then the numerically obtained time-dynamical expressions for $p_{2,3}$ converge to the steady state.

$$\frac{dq_1}{dt} + \left[i(\omega - \omega_{21}) + \frac{1}{\tau_2}\right] q_1 = \frac{iN\varepsilon_h''(\omega_{21})}{2\tau_2}\left[E_0^* - p_3^* - (1-\rho^3)p_2^*\right] \tag{4.1a}$$

$$\frac{dN}{dt} + \frac{N - N_0}{\tau_1} = \frac{1}{\tau_1}\Im\left\{q_1[E_0 - p_3 - (1-\rho^3)p_2]\right\} \tag{4.1b}$$

$$\frac{dq_2}{dt} - \frac{i\omega}{\omega^2(1-\varepsilon_m)+1}q_2 = -\frac{i\omega(1-\varepsilon_m)}{\omega^2(1-\varepsilon_m)+1}\left[E_0 - p_3 + \rho^3 p_2\right] \tag{4.1c}$$

$$\frac{d\sigma}{dt} - \frac{i\omega}{\omega^2(1-\varepsilon_m)+1}\sigma = -\frac{i\omega(1-\varepsilon_m)}{\omega^2(1-\varepsilon_m)+1}p_2 \tag{4.1d}$$

$$p_2 = \frac{(\varepsilon_b - 1)(E_0 - \rho^3 p_3) + q_2 - 2(q_1^* + \sigma)}{\varepsilon_b + 2 - \rho^3(\varepsilon_b - 1)} \tag{4.1e}$$

$$p_3 = \frac{(1-\varepsilon_3)(\varepsilon_b+2) + \rho^3(\varepsilon_b-1)(\varepsilon_3+2)}{(\varepsilon_b+2)(1+2\varepsilon_3) + 2\rho^3(\varepsilon_b-1)(1-\varepsilon_3)}E_0 + \tag{4.1f}$$

$$- \frac{6\rho^3 q_1^* + (1-\rho^3)\left[(\varepsilon_b+2)q_2 - 2\rho^3(\varepsilon_b-1)\sigma\right]}{(\varepsilon_b+2)(1+2\varepsilon_3) + 2\rho^3(\varepsilon_b-1)(1-\varepsilon_3)} \tag{4.1g}$$

4.1 An Experimentalist's Dream or: Fewer Gain for Thinner Shells

After showing that the steady state polarizability (α) in regions 2 and 3 is retrieved from the time-dynamical equations above, the dependency of $\alpha_3 = 4\pi\varepsilon_0\varepsilon_3 a_2^3\, p_3(t)/E_0$ on the thickness of the shell is studied. A plot of the polarizability in the outer region for three different values of $\rho = r_1/r_2$ and four different values of gain $\varepsilon_h''(\omega_{21})$ is shown in fig. 4.1.

The first observation that can be drawn is that the center of the plasmon in blue-shifted as ρ is increased. Furthermore, it is interesting to note that the morphology of the polarizability of

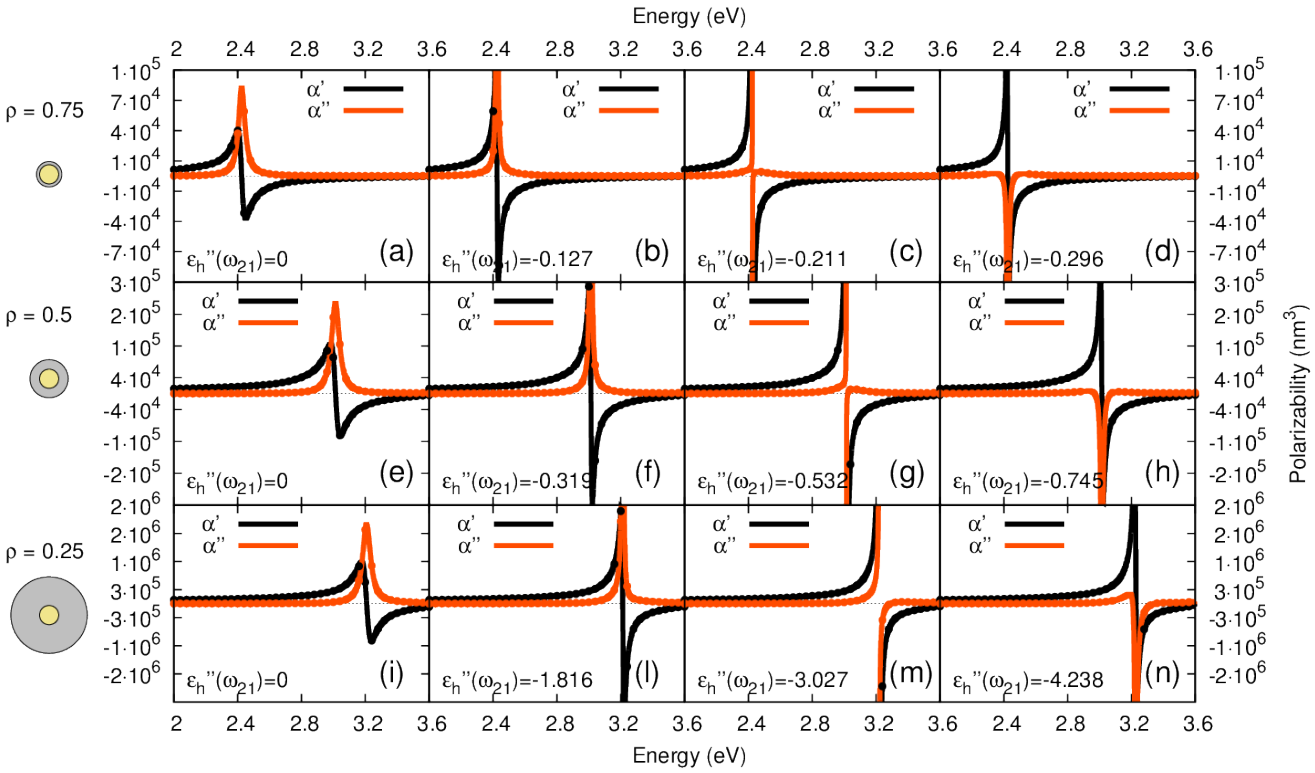

FIGURE 4.1: Metal Thickness dependency for different $\varepsilon_h''(\omega_{21})$.

shells of increasing thickness remains essentially the same if values of gain are increased (e.g. fig. 4.1[(b),(f),(l)]).

However, the most remarkable observation that can be drawn from fig. 4.1 is that the amount of gain required to obtain a singularity in the polarizability is less as ρ is increased (fig. 4.1[(c),(g), (m)]). Several experimental works report the production of metallic nanoshells with radii relationships of as high as $\rho = 0.9$ [67–70]. This means that a thinner nanoshell will be experimentally more feasible. Nonetheless, the next sections will consider a radii relationship $\rho = 0.5$, as no changes in morphology are present as ρ varies.

The results of the time-dynamical model of eqn. set 4.1 are presented as follows. The first step is to find if an instability exists for a zero external driving field ($E_0 = 0$), complete population inversion ($N = N_0 = 1$), and different gain values for active elements. If said instability appears then a spasing region is said to exist. Then, turning on the driving field, and still considering a complete population inversion, time-dynamical equations 4.1a, 4.1c, and 4.1d are solved numerically with a Runge-Kutta 4 algorithm. However, these solutions are only meaningful for small values of gain, since an "infinite" amplification will be seen for $\varepsilon_h''(\omega_{21})$ larger than the threshold amount of gain. Finally, in order to obtain the real picture, the depletion of the population inversion is considered (i.e. eqn. 4.1b is considered). To study this, a modification of the previous code is written.

4.2 Instabilities for Zero External Field and Spasing Threshold

Classical lasing is usually described as electromagnetic cavities that have negative dielectric loss (damping) due to population inversion in the molecules of the dielectric medium. Transition from a higher to a lower energy occurs in the form of stimulated emission. Electromagnetic oscillations in the cavity feed energy to the dielectric medium even when no external field is present, i.e. no external driving force is applied. This means that the system is described by "self-oscillations"[1] [72].

In the same way as self-oscillations are a characteristic of classical lasing, if a spasing region exists one would expect a self-oscillation in the absence of the external driving field ($E_0 = 0$), given that the amount of gain surpasses a given threshold. This situation is studied in a numerical way after assuming a complete population inversion ($N_0 = 1$) for the quantum emitters.

Due to the fact that no external field is applied, no fields are expected to be strong enough to deplete gain elements. This means that the right hand side of eqn. 4.1b will be negligible, and it is possible to state that $N = N_0$.

$$\frac{dq_1}{dt} + \left[i(\omega - \omega_{21}) + \frac{1}{\tau 2}\right] q_1 = -\frac{iN_0\varepsilon_h''(\omega_{21})}{2\tau_2}\left[p_3^* + (1-\rho^3)p_2^*\right] \tag{4.2a}$$

$$\frac{dq_2}{dt} - \frac{i\omega}{\omega^2(1-\varepsilon_m)+1} q_2 = \frac{i\omega(1-\varepsilon_m)}{\omega^2(1-\varepsilon_m)+1}\left[p_3 - \rho^3 p_2\right] \tag{4.2b}$$

$$\frac{d\sigma}{dt} - \frac{i\omega}{\omega^2(1-\varepsilon_m)+1}\sigma = -\frac{i\omega(1-\varepsilon_m)}{\omega^2(1-\varepsilon_m)+1} p_2 \tag{4.2c}$$

Since we are assuming a linear system, i.e. N is not time dependent, and no external field is applied, the coupled differential equations of eqn. set 4.2 will have exponential solutions of the form $e^{\lambda t}$. These solutions are expressed with three eigenvalues λ_i and three eigenvectors $\boldsymbol{c_i}$ as follows:

$$\begin{pmatrix} {q_1^*}^H \\ {q_2}^H \\ {\sigma}^H \end{pmatrix} = \begin{pmatrix} c_1^{(1)} \\ c_1^{(2)} \\ c_1^{(3)} \end{pmatrix} e^{\lambda_1 t} + \begin{pmatrix} c_2^{(1)} \\ c_2^{(2)} \\ c_2^{(3)} \end{pmatrix} e^{\lambda_2 t} + \begin{pmatrix} c_3^{(1)} \\ c_3^{(2)} \\ c_3^{(3)} \end{pmatrix} e^{\lambda_3 t}$$

These eigenvalues are obtained numerically, and they were all found to be frequency dependent and also depend on the amount of gain that is present in the inner region of the nanoshell (eqn. 4.1a). The amount of gain will be defined through the quantity $\varepsilon_h''(\omega_{21})$, and more gain is represented by a more negative value of $\varepsilon_h''(\omega_{21})$. The **real** part of the three eigenvalues ($\Re[\lambda_i]$) for different gain values are plotted for the frequency range $[2.7\,eV : 3.2\,eV]$ in fig. 4.2. The spasing instability will arise if at least one of the three eigenvalues have a positive real component. This will occur after a threshold amount of gain is reached.

For these calculations, and all subsequent ones, the solvent used (outer region) is water of $\varepsilon_w = 1.7689$, the background dielectric for the gain medium is silica of $\varepsilon_b = 2.1316$, and silver was modeled with an interpolation of experimental data of Johnson and Christy [73].

It is clear from fig. 4.2 that the spasing instability that was mentioned appears for the first time somewhere in the range $-\varepsilon_h''(\omega_{21}) = [0.5 : 0.55]$, as the real part of one eigenvalue becomes

[1] Self-oscillation is a "property of certain dynamical systems that gives rise to a variety of vibrations, both useful and destructive" [71].

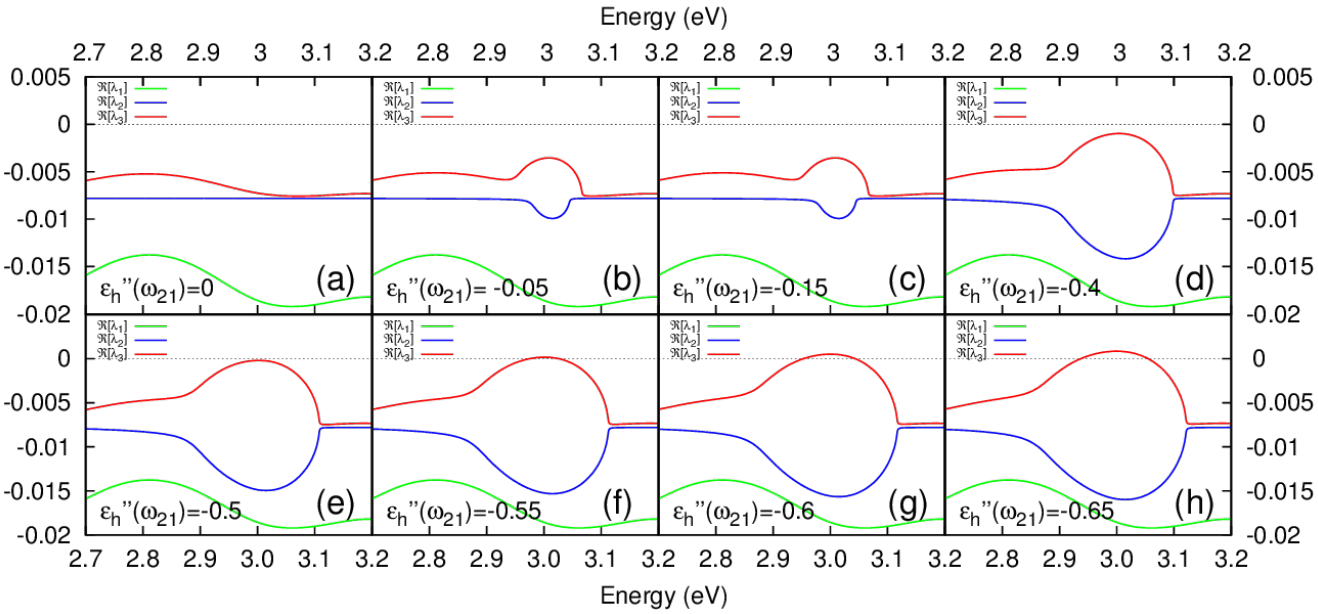

FIGURE 4.2: Eigenvalues for different $\varepsilon_h''(\omega_{21})$.

positive in a small region. This is observed in fig. 4.2(f). As the amount of gain is increased, the range over which $\Re[\lambda_3]$ is positive is broader, as shown in fig. 4.2(f, g, h).

In order to look for the threshold value of gain a plot of the amount of gain and the real part of the eigenvalues is made. The frequency chosen to do this study is the plasmon frequency for silver $\hbar\omega_p = 3.01296\ [eV]$, where $\Re[\lambda_3]$ is close to the maximum. In fig. 4.3 the threshold amount of gain is $\varepsilon_h''(\omega_{21}) = -0.532$. However, since the positive eigenvalue appears at a slightly smaller energy than $\hbar\omega_p$, the overall gain threshold is found to be $\varepsilon_h''(\omega_{21}) = -0.526$.

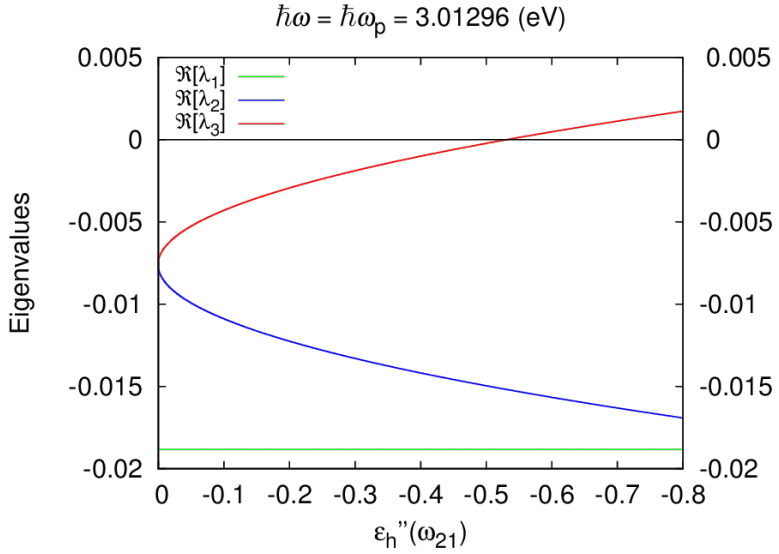

FIGURE 4.3: Eigenvalues as gain increases for $\hbar\omega = 3.0128[eV]$.

Emphasizing on the fact that a shell with radii relationship of $\rho = 0.75$ will have a lower gain threshold than one of $\rho = 0.5$, it was calculated that the gain threshold for the nanoshell of $\rho = 0.75$ is $\varepsilon_h''(\omega_{21}) = -0.211$. The shape of the real part of the eigenvalues is the same for

different values of ρ, but looking in the plasmon frequency for the respective radii relationship, for $\rho = 0.75$: $\hbar\omega_p = 2.425\ [eV]$.

The range where the real part of λ_3 has a positive sign is represented as an exponentially increasing function in time. As two eigenvalues have negative real components, after enough time, $e^{\lambda_{1,2}t}$ will reach zero. This means that ${q_1^*}^H$, ${q_2}^H$, and σ^H after enough time will depend exclusively on $e^{\lambda_3 t}$, and they will have values that approach infinity.

4.3 External Field Amplification - Linear Regime

Now the case for a non-zero external field $E_0 \neq 0$ being incident on the nanoshell will be considered. We start assuming that the amount of gain is below the gain threshold where the spasing instability appears. Since the amplification regime due to spasing has not appeared yet, no fields are expected to be strong enough, so we consider that the right hand side term $(\boldsymbol{E}_1 \cdot \boldsymbol{\Pi} - \boldsymbol{E}_1^* \cdot \boldsymbol{\Pi}^*) = 2\Im[\boldsymbol{E}_1 \cdot \boldsymbol{\Pi}]$ from eqn. 3.7b, which measures the depletion of the population inversion is negligible, meaning that $N = N_0$ at all times. A simplified system of equations arises as eqn. 4.1a becomes linear. The equations that govern the system in this "linear regime" are defined by eqn. set 4.3:

$$\frac{dq_1}{dt} + \left[i(\omega - \omega_{21}) + \frac{1}{\tau 2}\right] q_1 = \frac{iN_0\varepsilon_h''(\omega_{21})}{2\tau_2}\left[E_0^* - p_3^* - (1-\rho^3)p_2^*\right] \tag{4.3a}$$

$$\frac{dq_2}{dt} - \frac{i\omega}{\omega^2(1-\varepsilon_m)+1} q_2 = -\frac{i\omega(1-\varepsilon_m)}{\omega^2(1-\varepsilon_m)+1}\left[E_0 - p_3 + \rho^3 p_2\right] \tag{4.3b}$$

$$\frac{d\sigma}{dt} - \frac{i\omega}{\omega^2(1-\varepsilon_m)+1}\sigma = -\frac{i\omega(1-\varepsilon_m)}{\omega^2(1-\varepsilon_m)+1} p_2 \tag{4.3c}$$

After these considerations are made, a numerical code to solve the system in the linear regime is written. The solutions that are obtained through the numerical model are concisely summarized with the polarizability in the outer region after a relaxation time has passed:

$$\alpha_3 = 4\pi\varepsilon_0 a_2^3\, p_3(t)/E_0 \tag{4.4}$$

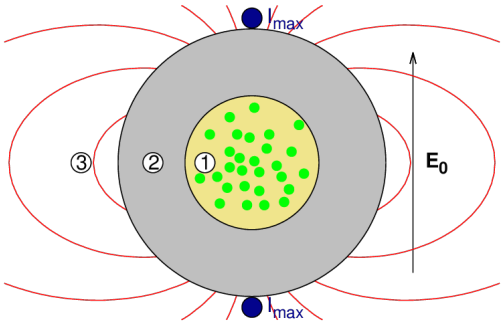

FIGURE 4.4: Position where $\boldsymbol{E}_3$'s intensity is maximized.

The intensity $I = |\boldsymbol{E}_3|^2$ of the outer field in the edge of the nanoshell (fig. 4.4) is obtained with eqn. set 3.16 and calculated with eqn. 4.5 for values of gain below and above the threshold gain for spasing instability. For values above the gain threshold this can be achieved with a

"perfect" pump, i.e. has infinite pumping rate ($\tau_1 \to 0$ in eqn. 4.1b). For values larger than the gain threshold, linear instabilities will arise. They are represented by an exponentially growing, infinite amplification (fig. 4.5(f,g,h)). Since a pump's rate cannot be infinite, when the amount of gain is larger than the threshold, the linear scenario lacks in physical meaning.

$$I(r,\theta) \sim E_0\, E_0^* \left[|\alpha_3|^2 \frac{1+3\cos^2\theta}{r^6} - 2\Re[\alpha_3]\frac{1-3\cos^2\theta}{r^3} \right] \tag{4.5}$$

$$\frac{I(r=a_2,\theta=0 \text{ or } \pi)}{I_0} = \frac{I_{max}}{I_0} \sim 1 + \frac{4|\alpha_3|^2}{a_2^6} - \frac{4\Re[\alpha_3]}{a_2^3} \tag{4.6}$$

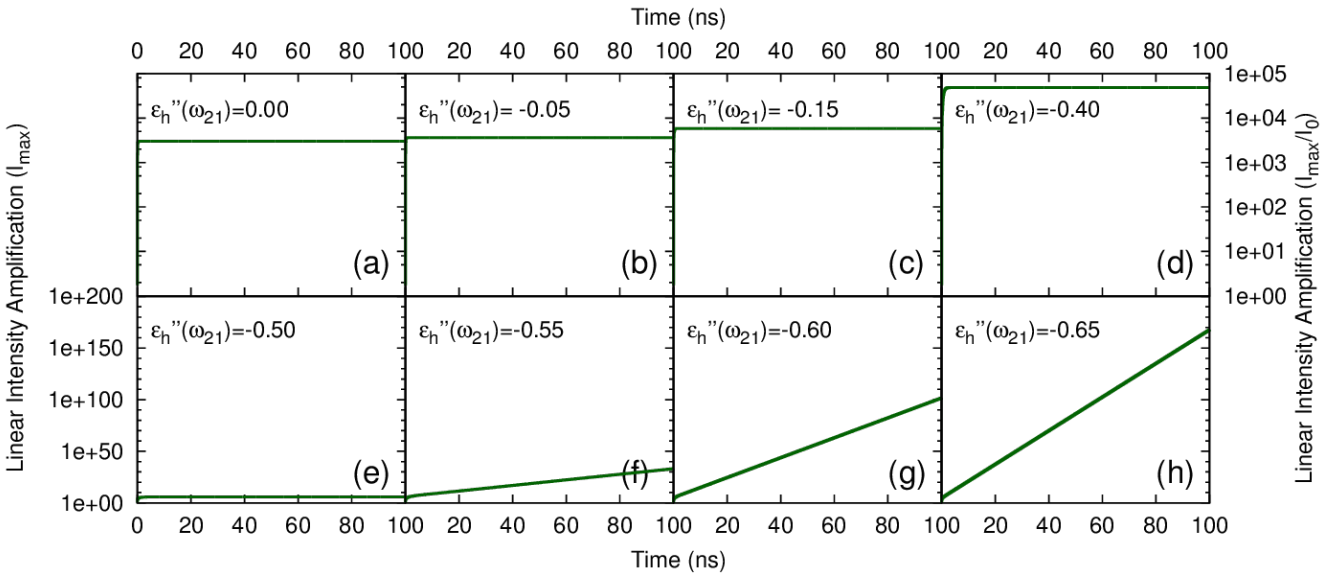

FIGURE 4.5: Temporal image of the maximum intensity amplification for different $\varepsilon_h''(\omega_{21})$ in the linear regime.

The results of the simulation for the linear regime are shown in fig. 4.6, where three things are being plotted. The red curve represents the real component of the eigenvalue λ_3. As it was shown before, $\Re[\lambda_3]$ turns positive for a given frequency range if the gain threshold ($\varepsilon_h''(\omega_{21}) = -0.526$) is reached. Additionally, the steady state maximum intensity amplification is plotted with a filled light-green curve. That is, the intensity amplification in $r = a_2$, $\theta = 0$ or π corresponding to the steady state polarizability:

$$\alpha_3^{ss} = 4\pi\varepsilon_3 a_2^3 \frac{(\varepsilon_m-\varepsilon_3)(\varepsilon_h+2\varepsilon_m)+\rho^3(\varepsilon_h-\varepsilon_m)(\varepsilon_3+2\varepsilon_m)}{(\varepsilon_m+2\varepsilon_3)(\varepsilon_h+2\varepsilon_m)+2\rho^3(\varepsilon_m-\varepsilon_3)(\varepsilon_h-\varepsilon_m)}$$

$$I(r=a_2,\theta=0\,\text{or}\,\pi) \sim 1 + \frac{4|\alpha_3^{ss}|^2}{a_2^6} - \frac{4\Re[\alpha_3^{ss}]}{a_2^3}$$

Finally, fig. 4.6 plots the maximum intensity amplification of the outer field for the linear case ($r = a_2$, $\theta = 0$ or π) with dark-green dots. It is clear that exactly for the values of gain where positive, real, eigenvalues exist, a linear instability appears (fig. 4.5(f,g,h) and fig. 4.6(f,g,h)).

The regions where a linear instability exists do not have their calculated value for I_{max}/I_0 because said value is characterized by non-stop growth (i.e. their values approach infinity - fig. 4.5(f,g,h)). Instead of that, their values are substituted with a yellow line.

We refer to the gain values that display no amplification in the form of a spasing instability (i.e. no yellow line exists) as the "linear amplification regime". In this regime, despite not having a spasing instability, partial loss compensation takes place, e.g. fig. 4.6(a-e).

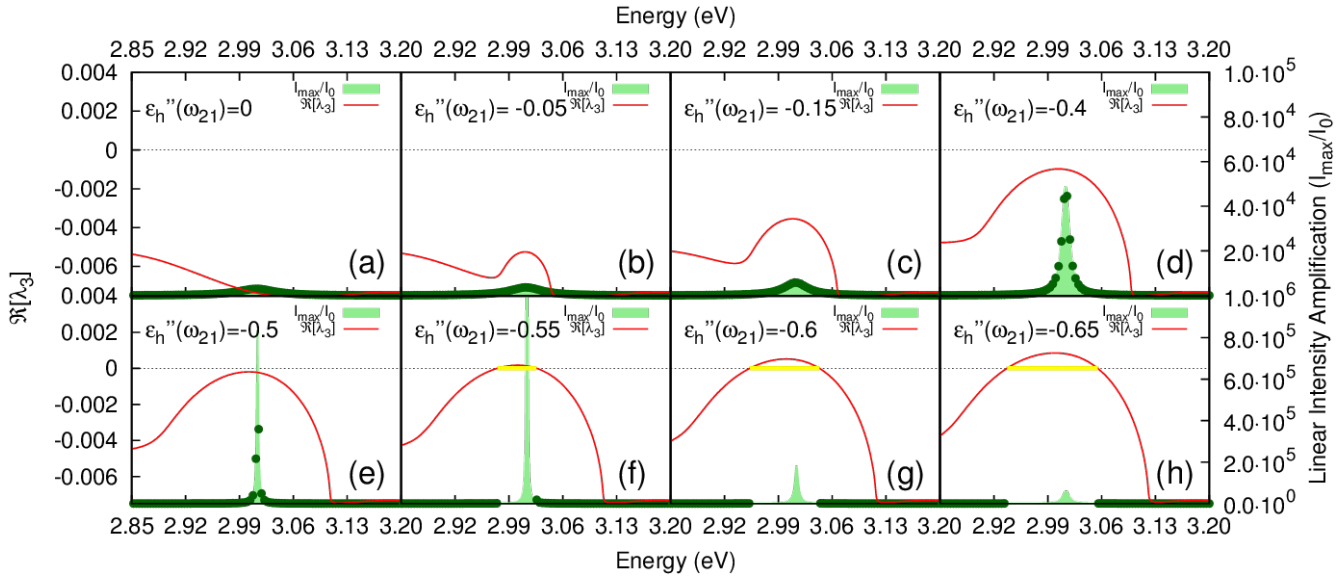

FIGURE 4.6: Maximum intensity amplification for different $\varepsilon_h''(\omega_{21})$ in the linear regime.

In order to understand the real behaviour of the system, the depletion of gain elements must be considered: dropping the assumption that the r.h.s. term of eqn. 4.1b is negligible leads to a time dependent population inversion, i.e. $N \neq N_0$. We call this the non-linear regime because eqn. 4.1a becomes non-linear. As a result, the linear amplification regime will remain unchanged (except for values of gain close to $\varepsilon_h''(\omega_{21}) = -0.526$, where the r.h.s term of eqn. 4.1b starts to become non-negligible), while for gain values larger than the gain threshold, the linear instabilities will make way to convergent values for the intensity amplification of the outer field.

4.4 Gain Depletion - Non-Linear Regime

This section looks at the full system of equations, eqn. set 4.7, which includes the time dependent population inversion. In this analysis, no assumptions are made regarding the amount of gain of the system. As a result, eqn. 4.7b, which takes into consideration the depletion of gain elements, will stabilize the intensity amplification to finite values. This will happen after a certain (frequency dependent) relaxation time, which is related to $\Re[\lambda_3]^{-1}$, and it will be described in detail in section 4.5.

$$\frac{dq_1}{dt} + \left[i(\omega - \omega_{21}) + \frac{1}{\tau_2}\right] q_1 = \frac{iN\varepsilon_h''(\omega_{21})}{2\tau_2}\left[E_0^* - p_3^* - (1-\rho^3)p_2^*\right] \tag{4.7a}$$

$$\frac{dN}{dt} + \frac{N - N_0}{\tau_1} = \frac{1}{\tau_1}\Im\left\{q_1[E_0 - p_3 - (1-\rho^3)p_2]\right\} \tag{4.7b}$$

$$\frac{dq_2}{dt} - \frac{i\omega}{\omega^2(1-\varepsilon_m)+1} q_2 = -\frac{i\omega(1-\varepsilon_m)}{\omega^2(1-\varepsilon_m)+1}\left[E_0 - p_3 + \rho^3 p_2\right] \tag{4.7c}$$

$$\frac{d\sigma}{dt} - \frac{i\omega}{\omega^2(1-\varepsilon_m)+1}\sigma = -\frac{i\omega(1-\varepsilon_m)}{\omega^2(1-\varepsilon_m)+1} p_2 \tag{4.7d}$$

As it was done in the previous section, the results of numerically solving the differential equations are summarized with the maximum intensity amplification for the field outside the nanoshell. The resultant intensity amplification, the steady state amplification, and $\Re[\lambda_3]$ for different values of gain are shown in fig. 4.7 with the same color codes as it was done for fig. 4.6.

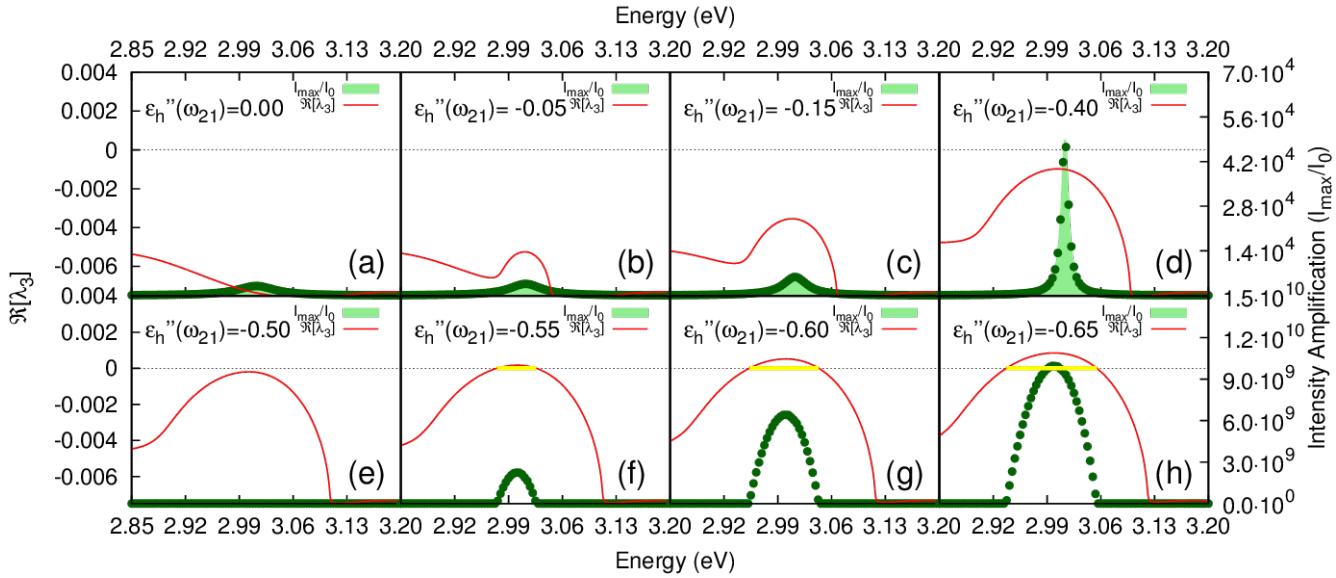

FIGURE 4.7: Maximum intensity amplification for different $\varepsilon_h''(\omega_{21})$ in the non-linear regime.

An important statement can be made regarding the pump that excites the gain elements. Its pumping rate, related to τ_1 in eqn. 4.7b, is that of a real pump - one that cannot create a complete population inversion regardless of the amount of gain; unlike the one that would be needed for the linear scenario outside the linear amplification regime.

The first observation that can be drawn from fig. 4.7 is that in the region where the real part of λ_3 becomes positive there is a very strong amplification of the field outside the nanoshell. This means that the strong intensity amplification appears exactly where the spasing instability occurs. In other words, a spaser appears! This confirms our claim that given a region where the real part of at least one eigenvalues becomes positive a spaser appears.

Another interesting feature of this system is that it decays extremely fast as we get farther away from the outer edge of the nanoshell. In fact, according to eqn. 4.5 the intensity amplification decays as r^{-6}. This strong localization of the external field is evidence that what is being

observed is a surface effect. However, due to the spasing nature of the amplification, there is also a strong far-field emission - "nanolasing".

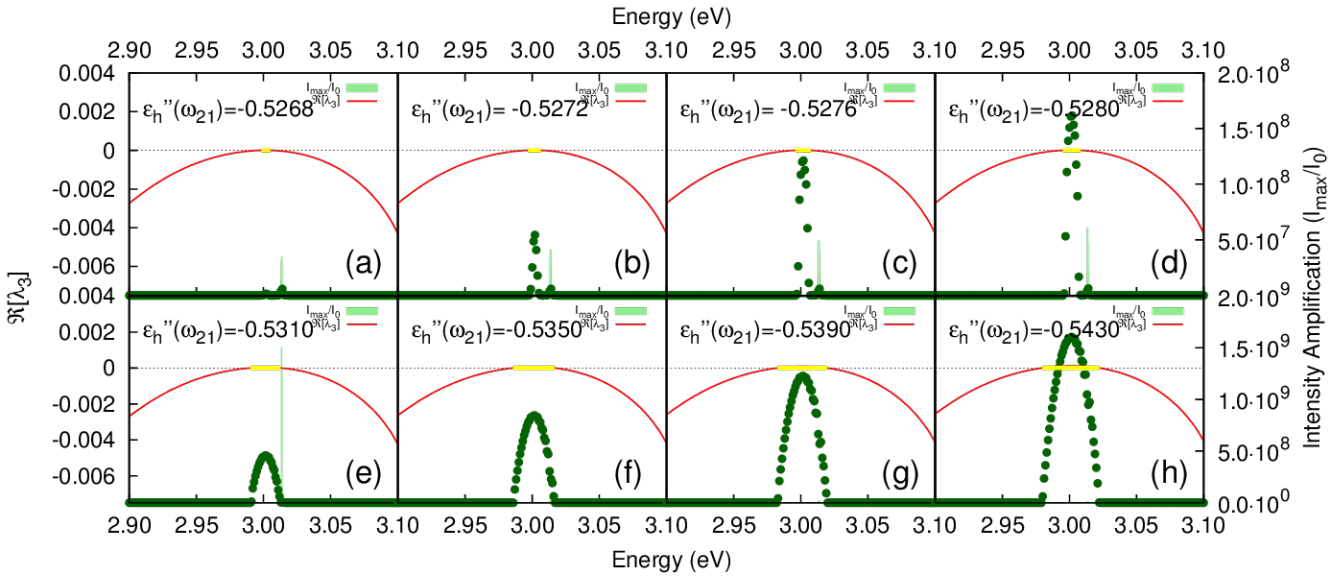

FIGURE 4.8: Two peaks of maximum intensity amplification for different $\varepsilon''_h(\omega_{21})$ in the non-linear regime.

A closer look at the transient regime where the amount of gain is just enough to obtain an instability shows two intensity peaks. One of these corresponds to the linear steady state peak and the other one is a "non-linear" peak. The latter "eats" the steady state peak when the amount of gain is increased. This can be observed in fig. 4.8, and in fig. 4.7(e, f, g, h) where the "non-linear" peak has completely overshadowed the linear steady state peak.

4.5 Temporal Evolution: Non-Linear Regime

The non-linear instabilities that have been observed show a very strong field amplification outside the nanoshell in a very narrow emission bandwidth ($\Delta\lambda \sim 7\ [nm]$) above a threshold amount of gain. This section is interested in their time dependency. This will help shed a light on the physical meaning of this amplification, that we have labeled as a spaser. The time evolution of the population inversion (purple line) and the maximum intensity amplification (dark-green line) in the plasmon frequency for silver ($\hbar\omega = 3.013\ [eV]$) for different values of gain is shown in fig. 4.9 and fig. 4.10. The latter corresponds to the end of the "two peak" region, and clearly displays the rapid intensity growth that is also observed in fig. 4.8.

The temporal curves of figs. 4.9 and 4.10 display typical relaxation times which depend on both the amount of gain and the frequency that is being considered. Since the growth of the intensity amplification is dominated by the linear regime, and limited by the depletion of gain elements, we should expect the relaxation times to be governed by $\tau_{lin} = \Re[\lambda_3]^{-1}$ for values of gain above the threshold in the frequency region where the real part of λ_3 is positive[2].

Figures 4.9 and 4.10 show the gain-dependent stabilization times at the plasmon frequency. These stabilization times are extremely low at first (below the threshold amount of gain in the

[2]The inverse of the real part of λ_3 will only have positive values (and physical meaning as a relaxation time) in the range where $\Re[\lambda_3] > 0$, i.e. the spasing instability.

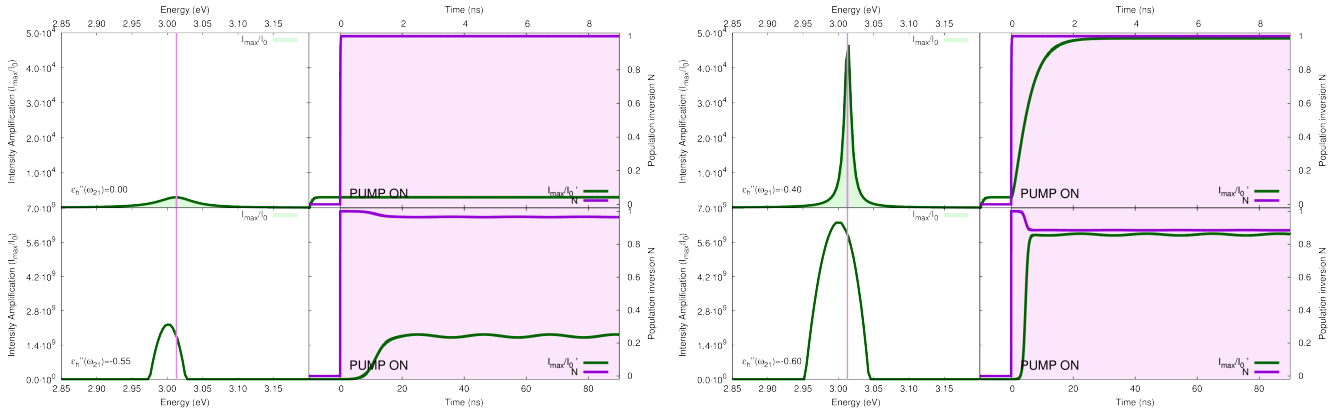

FIGURE 4.9: Temporal profile of the population inversion and maximum intensity amplification for different values of $\varepsilon_h''(\omega_{21})$.

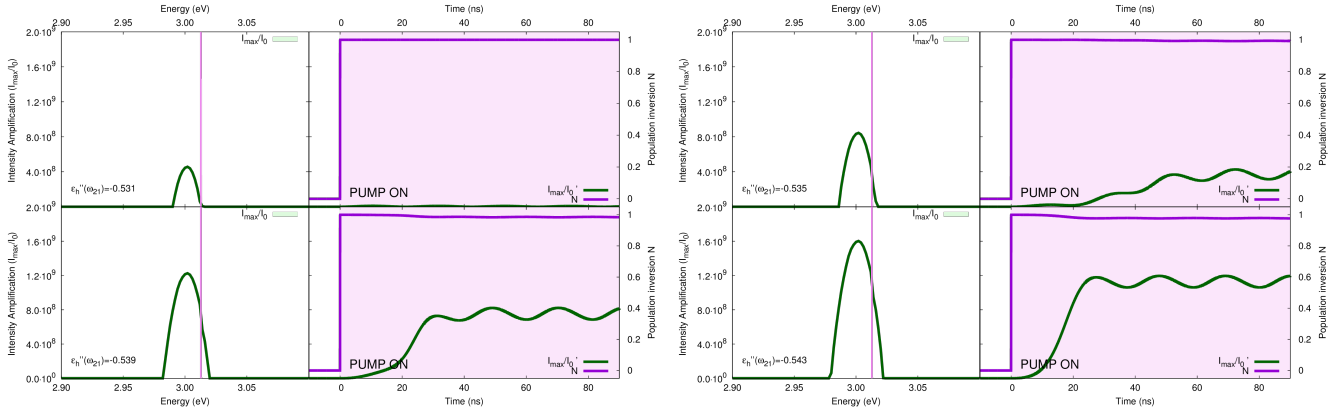

FIGURE 4.10: Temporal profile of the population inversion and maximum intensity amplification for different values of $\varepsilon_h''(\omega_{21})$ very close to the gain threshold.

plasmon frequency: $\varepsilon_h''(\omega_{21}) = -0.532$), i.e. fast stabilization. Exactly for $\varepsilon_h''(\omega_{21}) = -0.532$ the stabilization time is extremely long, as $\tau_{lin} = \Re[\lambda_3]^{-1}$ approaches infinity.

On the other hand, for energies higher than $\hbar\omega_p$ the stabilization times will become constantly slower when the gain is equal $\varepsilon_h''(\omega_{21}) = -0.532$ (spasing instability gain threshold for the plasmon frequency). In the same way, the time required for stabilization in the plasmon frequency becomes smaller as more gain is added, as shown in fig. 4.10. It is interesting to note that after the plasmon frequency threshold amount of gain has been reached the maximum intensity amplification in ω_p is described by oscillations with the same period ($\sim 20\ [nm]$).

The temporal profile for the intensity, together with the frequency profile that were shown in figs. 4.8 and 4.10 are considerably similar to those presented in experimental papers that describe a spaser response. [74,75] A theoretical work by Stockman and an experimental work show the same temporal profile for the population inversion of fig. 4.10 as well. [76,77] These similarities between the calculated response of the nanoshell and previous experimental and theoretical work suggest that the amplification that is being observed is in fact that of a spaser. Further work on this nanoshell could be to obtain the relation between the pump intensity and the maximum intensity amplification. If this shows a linear growth followed by a stable region, it could be vigorously stated that the response that is being observed is in fact a spaser. [74,78, 79]

4.6 Conclusions

A silver nanoshell, illuminated by an external probe field, was filled with dielectric and gain, excited with a pump field was studied. Classically modeling the metal (Drude model) and the gain elements in a quantum mechanical way (optical-Bloch), a set of equations describing the system was obtained (eqn. set 4.1). Finally, these equations were solved with a numerical model and their results expressed via the maximum intensity amplification of the resultant field just outside the nanoshell ($r = a_2, \theta = 0$ or π).

When looking at the eigenvalues of eqn. set 4.1 for zero external field, a positive real eigenvalue can be observed after a sufficiently high amount of gain (fig. 4.2). This means that an exponential growth in time will occur, and, if the depletion of the gain elements is not considered, the maximum intensity amplification will grow forever, as fig. 4.6 suggests. Moreover, even when the depletion of gain elements (eqn. 4.1b) is considered, the steady-state intensity amplification is surprisingly large in the region where a real eigenvalue is positive.

It is worth noting that the linewidths observed after the threshold amount of gain are considerably thin, however becoming larger as more gain is added. Thus in order to obtain a sharp emission line and a strong amplification, an amount of gain corresponding to $\varepsilon_h''(\omega_{21}) \sim -0.543$ would be adequate as it would have $\Delta\lambda \sim 6\ [nm]$ and $I_{max}/I_0 \sim 10^9$.

Furthermore, as it was explained in the previous section, the results obtained for $\varepsilon_h''(\omega_{21}) = -0.543$ are extremely encouraging as they can be compared to those of [74–79], where spasers have been accounted for (both theoretically and experimentally). From this, it is stated that the nanoshell geometry that is under study presents a spaser response when the dielectric inside the shell is doped with enough gain material.

The experimental realization of this device would mean a wide range of applications. For example, if the silver nanoshell spaser amplifies enough it could destroy malign cells in the same way that has been done in [75, 80]. Potentially, as it was shown this device offers loss-compensation that could be used in applications such as metamaterials or super-lenses by tuning the responses through the radii relationship ρ, the amount of gain $\varepsilon_h''(\omega_{21})$, and the pumping rate W. Furthermore, is is possible that the nanoshell could become an alternative for an optical nano-transistor, as it has been theorized that spasers can act as "an ultra-fast nanoamplifier - the optical counterpart of the MOSFET" [76].

Appendix A

Density Matrix and Optical-Bloch Equations

Consider a quantum system that is defined by an arbitrary vector, $|\psi\rangle$, which is a function of the generalized coordinates q_k. This system's evolution is described by a hamiltonian, $H(q_k, p_k, t)$, function of the generalized coordinates, generalized momenta (p_k), and time.
From this, Schrödinger's equation is described by eqn. A.1.

$$H|\psi\rangle = i\hbar \frac{\partial}{\partial t}|\psi\rangle \tag{A.1}$$

The state of the system can be written as a linear combination of the stationary solutions of the hamiltonian, $|\phi_i\rangle$, each related to a certain energy, E_i, satisfying eqn. A.2 This linear combination can be written as eqn. A.3.

$$H|\phi_i\rangle = E_i|\phi_i\rangle \tag{A.2}$$

$$|\psi(q_k, t)\rangle = \sum_i c_i(t)\,|\phi_i(q_k)\rangle \tag{A.3}$$

Since the basis that was chosen is a complete orthonormal one, eqn. A.4 must be fulfilled. The abreviation $H_{ji} = \langle\phi_j|H|\phi_i\rangle$ will be used. This, along with eqns. A.2 and A.4 provides $H_{ji} = E_i\delta_{ji}$.

$$\langle\phi_j|\phi_i\rangle = \delta_{ij} \tag{A.4}$$

Each eigenstate, ϕ_i, comes with a particular probability of occupation, p_i, given by $|c_i|^2$. Since the basis of eigenvectors that has been chosen must make a complete orthonormal basis, then the sum of probabilities must be 1. By multiplying eqn. A.3 in both sides by $\langle\phi_j|$, the following expression is obtained:

$$\langle\phi_j|\psi\rangle = \sum_i c_i(t)\langle\phi_j|\phi_i\rangle = \sum_i c_i(t)\delta_{ij}$$

From this expression it is possible to determine the value of each coefficient, $c_j(t)$:

$$c_j = \langle\phi_j|\psi\rangle$$

Now, substituting the expression for ψ in eqn. A.3 in Schrödinger's equation:

$$i\hbar \sum_i \frac{dc_i}{dt}|\phi_i\rangle = H \sum_i c_i|\phi_i\rangle$$

Multiplying this expression by $\langle\phi_j|$, and applying eqn. A.4:

$$i\hbar \frac{dc_j}{dt} = \sum_i H_{ji}c_i$$

From here, two equations are obtained:

$$\frac{dc_i}{dt} = \frac{1}{i\hbar}\sum_k H_{ik}c_k \tag{A.5}$$

$$\frac{dc_j^*}{dt} = -\frac{1}{i\hbar}\sum_k H_{jk}^*c_k^* \tag{A.6}$$

A.1 The Density Matrix (in the flesh)

The following formalism is particularly useful when dealing with quantum states in a mixed state, like a three-level system laser. The density matrix is defined as $\rho_{ij} = c_i c_j^*$, and it is a hermitian matrix. The diagonal elements of the density matrix, ρ_{ii}, determine the probability that the system is in the i^{th} state. This means that the trace of the density matrix is 1. The elements of the density matrix that lay outside the diagonal, $\rho_{ij}, i \neq j$, represent the probability amplitude of the system transitioning from state i to state j. Using A.5 and A.6 it is possible to determine how the density matrix depends on time.

$$\frac{d\rho_{ij}}{dt} = \frac{dc_i}{dt}c_j^* + c_i\frac{dc_j^*}{dt}$$

$$\frac{d\rho_{ij}}{dt} = \frac{1}{i\hbar}\sum_k \left(H_{ik}c_k c_j^* - H_{jk}^* c_i c_k^*\right) \tag{A.7}$$

Since the hamiltonian is a hermitian operator, $H_{jk}^* = H_{kj}$, and A.7 can be rewritten as:

$$\frac{d\rho_{ij}}{dt} = \frac{1}{i\hbar}\sum_k \left(H_{ik}\rho_{kj} - \rho_{ik}H_{kj}\right)$$

$$\frac{d\rho}{dt} = -\frac{i}{\hbar}\left[H, \rho\right] \tag{A.8}$$

This is perfectly well formulated except in the particular case when the density matrix depends explicitly on time. [81] For this analysis the time dependent wave function $|\psi(t)\rangle$ is considered. In terms of the time evolution operator, $U(t, t_0)$, the time dependent wave function can be expressed as the evolution of its state in $t = t_0$:

$$|\psi(t)\rangle \;=\; U(t,t_0)\,|\psi(t_0)\rangle, \qquad\qquad where: \quad U(t=t_0,t_0)=1 \tag{A.9}$$

Including this in Schrödinger's equation shows how the time evolution operator relates with the system's hamiltonian:

$$i\hbar\frac{d}{dt}|\psi(t)\rangle \;=\; H|\psi(t)\rangle$$

$$i\hbar\left[\frac{\partial U(t,t_0)}{\partial t}\,|\psi(t_0)\rangle \;+\; U(t,t_0)\frac{\partial}{\partial t}|\psi(t_0)\rangle\right] \;=\; H\,U(t,t_0)\,|\psi(t_0)\rangle$$

Since the initial state of the particle is independent of time:

$$i\hbar\frac{\partial U(t,t_0)}{\partial t}|\psi(t_0)\rangle \;=\; H\,U(t,t_0)|\psi(t_0)\rangle \tag{A.10}$$

Preforming a simple integration the relationship between the time evolution operator and the hamiltonian is obtained to be:

$$U(t,t_0) \;=\; e^{\frac{1}{i\hbar}H\,(t-t_0)} \tag{A.11}$$

Now an arbitrary operator, D, is considered. It evolves when the time dependent wave function, $|\psi(t)\rangle$, evolves as is described in eqn. A.9:

$$\begin{aligned}\langle\psi(t)|D|\psi(t)\rangle \;&=\; \langle\psi(t_0)|U^\dagger\,D\,U|\psi(t_0)\rangle\\ &=\; \langle\psi(t_0)|D_0|\psi(t_0)\rangle\\ D_0 \;&=\; U^\dagger\,D\,U\end{aligned}$$

Since the time evolution operator is unitary ($U^\dagger U \;=\; 1$), D can be expressed in terms of the evolution operator and D_0:

$$D \;=\; U\,D_0\,U^\dagger \tag{A.12}$$

Differentiating this in time, applying eqn. A.10 and its conjugate:

$$\begin{aligned}\frac{d\,D}{dt} \;&=\; \frac{\partial\,U}{\partial t}\,D_0\,U^\dagger \;+U\,D_0\,\frac{\partial\,U^\dagger}{\partial t} \;+\; U\,\frac{\partial D_0}{\partial t}\,U^\dagger\\ &=\; \frac{1}{i\hbar}\left[H\,U\,D_0\,U^\dagger \;+\; U\,D_0\,\left(-U^\dagger\,H\right)\right] \;+\; \frac{\partial D}{\partial t}\\ &=\; \frac{1}{i\hbar}\left[H\,D \;-\; D\,H\right] \;+\; \frac{\partial D}{\partial t}\\ &=\; \frac{1}{i\hbar}\left[H,D\right] \;+\; \frac{\partial D}{\partial t}\end{aligned}$$

Considering the density matrix the equation that is obtained is usually referred to as Liouville's equation:

$$\frac{d\rho}{dt} \;=\; \frac{1}{i\hbar}\left[H,\rho\right] \;+\; \left(\frac{\partial\rho}{\partial t}\right) \tag{A.13}$$

A.2 Optical Bloch

This appendix shows the particular case of the interaction of an electric field with gain elements, modeled as a two-level system, in a thermal bath with the optical-Bloch formalism. For the case of a two-level system alone, the hamiltonian can be written as eqn. A.14, where the eigenstates correspond to the ground state and the first excited state, $|g\rangle$ and $|e\rangle$ respectively. Each of this states has an associated eigenenergy, E_g and E_e, Fig. A.1.. These can be expressed as $\hbar\omega_g$ and $\hbar\omega_e$.

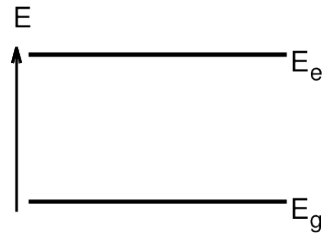

FIGURE A.1: Two-Level System.

$$H_0 = \hbar\omega_g|g\rangle\langle g| + \hbar\omega_e|e\rangle\langle e| \tag{A.14}$$

Next, the hamiltonian of the electric field is expressed in the basis of the unperturbed hamiltonian, H_0. The hamiltonian of an atom with dipole moment $\widehat{\mu}$ (eqn. A.15) in an electric field $\widehat{E} = \vec{E}\,\widehat{I}$ is defined as $H_1 = -\widehat{\mu}\,\widehat{E}$.[1] Considering a linearly polarized electric field and $\boldsymbol{\mu} = \mu_{12}(|g\rangle\langle e| + |e\rangle\langle g|)$, [82] the interaction hamiltonian can be rewritten as eqn. A.16.

$$\widehat{\mu} = \begin{pmatrix} 0 & \mu_{12} \\ \mu_{21} & 0 \end{pmatrix} = \vec{\mu}\begin{pmatrix} 0 & 1 \\ 1 & 0 \end{pmatrix} \tag{A.15}$$

$$H_1 = -\left(|g\rangle\langle e| + |e\rangle\langle g|\right)\vec{\mu}\cdot\vec{E} \tag{A.16}$$

Considering $H = H_0 + H_1$ as the complete hamiltonian for the system, Liouville's equation (A.13) is expressed as:

$$\frac{\rho_{mn}}{dt} = \frac{1}{i\hbar}[H,\rho]_{mn} + \left(\frac{\partial\rho}{\partial t}\right)_{mn} \tag{A.17}$$

For a system with quantum gain elements in the presence of a time dependent electric field and a phenomenological pump with a rate of W that drives population in the ground state to the first excited state. This system is represented as existing in a thermal bath and has energy and phase relaxation times of $\tilde{\tau_1}$ and τ_2 due to interaction with the thermostat. This means that the last term in Liouville's equation can be written as:

$$\left(\frac{\partial\rho}{\partial t}\right)_{mn} = -\frac{\rho_{mn} - \rho_{mn}^{(th)}}{T_{mn}}$$

$$\frac{1}{T_{mn}} = \left[\frac{1}{\tau_{mn}} + W\delta_{mn}\right]$$

[1] $\widehat{I}$ is the identity matrix; $\widehat{I} = \delta_{ij}$.

Here, the elements $\rho_{mn}^{(th)}$ correspond to the thermal equilibrium value of the density matrix, and it is constant. The off diagonal elements of T_{mn} are equal between each other, $T_{eg} = T_{ge} = \tau_2$, and $\tau_{nn} = \tau_{mm} = \tilde{\tau_1}$. The commutator between the complete hamiltonian, H, and the density matrix is calculated. This leads to the following equation:

$$\begin{pmatrix} \frac{d\rho_{gg}}{dt} & \frac{d\rho_{ge}}{dt} \\ \frac{d\rho_{eg}}{dt} & \frac{d\rho_{ee}}{dt} \end{pmatrix} = \frac{1}{i\hbar} \begin{pmatrix} (\rho_{ge} - \rho_{eg})\boldsymbol{\mu} \cdot \boldsymbol{E} & -\hbar\omega_{eg}\rho_{ge} - (\rho_{ee} - \rho_{gg})\boldsymbol{\mu} \cdot \boldsymbol{E} \\ \hbar\omega_{eg}\rho_{eg} + (\rho_{ee} - \rho_{gg})\boldsymbol{\mu} \cdot \boldsymbol{E} & -(\rho_{ge} - \rho_{eg})\boldsymbol{\mu} \cdot \boldsymbol{E} \end{pmatrix} + \\ + \begin{pmatrix} -\left(\rho_{gg} - \rho_{gg}^{(th)}\right)\left[\frac{1}{\tilde{\tau_1}} + W\right] & -\frac{\rho_{ge}}{\tau_2} \\ -\frac{\rho_{eg}}{\tau_2} & -\left(\rho_{ee} - \rho_{ee}^{(th)}\right)\left[\frac{1}{\tilde{\tau_1}} + W\right] \end{pmatrix} \tag{A.18}$$

In the previous equation, ω_{eg} is the difference in frequency of the excited state and the ground state, $\hbar\omega_{eg} = E_e - E_g$. To make things less cumbersome the variable τ_1 is introduced, where:

$$\frac{1}{\tau_1} = \frac{1}{\tilde{\tau_1}} + W$$

This leads to equations of motion for the matrix elements of the density matrix:

$$\begin{aligned} \frac{d\rho_{ge}}{dt} - \left(i\omega_{eg} - \frac{1}{\tau_2}\right)\rho_{ge} &= \frac{iN\boldsymbol{\mu} \cdot \boldsymbol{E}}{\hbar} \\ \frac{d\rho_{ee}}{dt} + \frac{\rho_{ee} - \rho_{ee}^{(th)}}{\tau_1} &= \frac{i(\rho_{ge} - \rho_{eg})\boldsymbol{\mu} \cdot \boldsymbol{E}}{\hbar} \\ \frac{d\rho_{gg}}{dt} + \frac{\rho_{gg} - \rho_{gg}^{(th)}}{\tau_1} &= -\frac{i(\rho_{ge} - \rho_{eg})\boldsymbol{\mu} \cdot \boldsymbol{E}}{\hbar} \end{aligned} \tag{A.19}$$

Now the population inversion is defined as $N = \rho_{ee} - \rho_{gg}$, and its equation of motion is obtained. Defining $N_0 = \rho_{ee}^{(th)} - \rho_{gg}^{(th)}$ as the population inversion at thermal equilibrium, eqn. A.20 arises:

$$\frac{dN}{dt} + \frac{N - N_0}{\tau_1} = \frac{2i(\rho_{ge} - \rho_{eg})\boldsymbol{\mu} \cdot \boldsymbol{E}}{\hbar} \tag{A.20}$$

Further explanations on the density matrix and optical-Bloch equations can be found in [82].

A.3 Gain Permittivity

Starting from eqn. set A.21 (obtained from chapter 3) it is possible to obtain the electric permittivity of the gain material that is being modeled through the two-level system optical-Bloch equations.

$$\frac{d\boldsymbol{\Pi}}{dt} + \left[i(\omega - \omega_{21}) - \frac{1}{\tau_2}\right]\boldsymbol{\Pi} = \frac{inN\,\boldsymbol{E}_1^*}{6\hbar} \tag{A.21a}$$

$$\frac{dN}{dt} + \frac{N - N_0}{\tau_1} = -\frac{2\Im[\boldsymbol{E}_1 \cdot \boldsymbol{\Pi}]}{n\hbar} \tag{A.21b}$$

$$\frac{d\boldsymbol{P}_2}{dt} - \frac{\omega^2 + 2i\gamma\omega}{2(\gamma - i\omega)}\boldsymbol{P}_2 = \frac{\varepsilon_0\omega_p^2}{2(\gamma - i\omega)}\boldsymbol{E}_2 \tag{A.21c}$$

The polarization density in the nanoshell's inner region is: $\boldsymbol{P}_1 = \varepsilon_0\chi_b\boldsymbol{E}_1 + 2\boldsymbol{\Pi}^*$. Considering the steady state regime for the polarization density of the gain elements $\left(\frac{d\boldsymbol{\Pi}}{dt} = 0\right)$ and defining $\Delta/2 = 1/\tau$ leads to:

$$\boldsymbol{\Pi} = \frac{in\mu^2 N\boldsymbol{E}_1^*}{6\hbar\left[i(\omega - \omega_{21}) + \frac{\Delta}{2}\right]} = \frac{n\mu^2 N\boldsymbol{E}_1^*}{3\hbar\left[2(\omega - \omega_{21}) - i\Delta\right]} \tag{A.22}$$

Taking the complex conjugate:

$$\boldsymbol{\Pi}^* = \frac{n\mu^2 N\boldsymbol{E}_1}{3\hbar\left[2(\omega - \omega_{21}) + i\Delta\right]}$$

Using this into the equation for the polarization density in region 1 of the nanoshell provides the following equation:

$$\boldsymbol{P}_1 = \varepsilon_0\left\{\chi_b + \frac{2n\mu^2 N}{3\hbar\varepsilon_0[2(\omega - \omega_{21}) + i\Delta]}\right\}\boldsymbol{E}_1$$

This gives the relative electric permittivity of the host medium (background and gain) since $\varepsilon_h = 1 + \chi_h$.

$$\varepsilon_h(\omega) = \varepsilon_b + \frac{2n\mu^2 N}{3\hbar\varepsilon_0[2(\omega - \omega_{21}) + i\Delta]} \tag{A.23}$$

When considering the linear case, the population inversion of the system goes to the population inversion imposed by the thermal bath, i.e. $N \to N_0$. We look at the imaginary component of ε_h when $\omega = \omega_{21}$.

$$\varepsilon_h''(\omega_{21}) = -\frac{2nN_0\mu^2}{3\hbar\varepsilon_0\Delta} \tag{A.24}$$

Now, eqn. A.23 is rewritten for the linear case with the use of eqn. A.24:

$$\varepsilon_h(\omega) = \varepsilon_b - \frac{\varepsilon_h''(\omega_{21})\Delta}{2(\omega-\omega_{21})+i\Delta} \tag{A.25}$$

For the non-linear steady state solution where $N \neq N_0$ a similar approach can be made. Equation A.21b becomes:

$$N = N_0 - \frac{2\tau_1 \Im[\boldsymbol{E}_1 \cdot \boldsymbol{\Pi}]}{n\hbar}$$

From eqn. A.22 this results in:

$$N = N_0 - \frac{2\tau_1 \mu^2 E_1^2 \Delta}{3\hbar^2[4(\omega-\omega_{21})^2+\Delta^2]} N$$

After some algebra this results in the following expression for the population inversion:

$$N = \frac{4(\omega-\omega_{21})^2 + \Delta^2}{4(\omega-\omega_{21})^2+\Delta^2\left[1+\frac{\tau_1\tau_2\mu^2E_1^2}{3\hbar^2}\right]} N_0 \tag{A.26}$$

Now, a saturation field is defined as $E_{sat}^2 = \frac{3\hbar^2}{\tau_1\tau_2\mu^2}$, which allows for eqn. A.26 to be recast as:

$$N = \frac{4(\omega-\omega_{21})^2 + \Delta^2}{4(\omega-\omega_{21})^2+\Delta^2\left[1+\left(\frac{E_1}{E_{sat}}\right)^2\right]} N_0$$

Replacing this N in the equation for the host relative electric permittivity, eqn. A.23, leads to:

$$\varepsilon_h(\omega) = \varepsilon_b - \frac{2n\mu^2 N_0}{3\hbar\varepsilon_0} \frac{2(\omega-\omega_{21})-i\Delta}{4(\omega-\omega_{21})^2+\Delta^2\left[1+\left(\frac{E_1}{E_{sat}}\right)^2\right]}$$

Which finally leads to the non linear steady state relative electric permittivity for the host:

$$\varepsilon_h(\omega) = \varepsilon_b + \varepsilon_h''(\omega_{21})\Delta \frac{2(\omega-\omega_{21})-i\Delta}{4(\omega-\omega_{21})^2+\Delta^2\left[1+\left(\frac{E_1}{E_{sat}}\right)^2\right]} \tag{A.27}$$

Where the saturation effect, when the external field becomes too large is included for the gain elements.

Appendix B

Classical (Steady State) Polarizability

B.1 Nanoshell Multipolar Model

Considering a curl-less electric field in each region, i.e. no time dependent magnetic field, the electric field can be written in terms of the electric potential, eqn. B.1.

$$\boldsymbol{E}_i \;=\; -\boldsymbol{\nabla}\,\phi_i \tag{B.1}$$

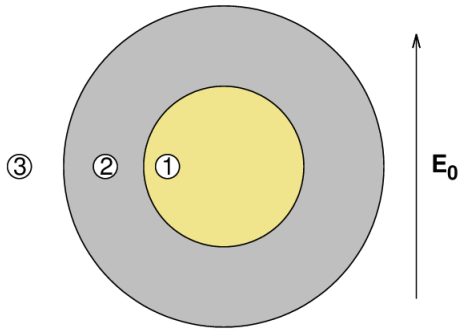

FIGURE B.1: Nanoshell Geometry without gain.

Using the quasistatic approximation ($a_2 << \lambda$, where $\lambda \approx 500\ [nm]$ is the wavelength of the external exciting field), *Laplace's equation* is met in all three regions. Since eqns. B.2, where ϕ_i is the electric potential in the i^{th} region, are met, and a uniform external field $\boldsymbol{E}_{ext} = E_0\,\hat{\boldsymbol{z}}$ would provide axial symmetry, it is possible to write ϕ_i through the Legendre polynomials. [50]

$$\nabla^2\phi_i \;=\; 0 \tag{B.2}$$

$$\phi^{(i)}(r,\theta) \;=\; \sum_{\ell=0}^{\infty}\left[\tilde{p}_\ell^{(i)}\,r^\ell + \frac{p_\ell^{(i)}}{r^{\ell+1}}\right]P_\ell(\cos\theta) \tag{B.3}$$

Over these solutions for the electric potential certain boundary conditions need to be made, as well as regularity conditions. In order for ϕ_1 to be finite in $r = 0$, $p_l^{(1)}$ needs to be 0 for every l (B.4). The electric field when $r \to \infty$ has to connect with the uniform external field, $|E_0|$, (B.5).

Additionally, the electric potential must be continuous while crossing the interface between two media. In other words, eqns. B.6. These last conditions of eqns. B.7 result in eqns.B.8.

$$\phi_1\left(r,\theta\right) = \sum_{\ell=0}^{\infty} \tilde{p}_\ell^{(1)}\, r^\ell\, P_\ell(\cos\theta) \tag{B.4}$$

$$\phi_3\left(r,\theta\right) = \sum_{\ell=0}^{\infty} \left[\frac{p_\ell^{(3)}}{r^{\ell+1}} - r\, E_0\, \delta_{\ell,1}\right] P_\ell(\cos\theta) \tag{B.5}$$

$$\phi_1(a_1,\theta) = \phi_2(a_1,\theta) \qquad\qquad \phi_2(a_2,\theta) = \phi_3(a_2,\theta) \tag{B.6}$$

$$\tilde{p}_\ell^{(1)} = \frac{p_\ell^{(2)}}{a_1^{2\ell+1}} + \tilde{p}_\ell^{(2)} \tag{B.7}$$

$$\tilde{p}_\ell^{(2)} = \frac{p_\ell^{(3)} - p_\ell^{(2)}}{a_2^{2\ell+1}} - E_0\, \delta_{\ell,1} \tag{B.8}$$

The relation between the smaller radius and the larger radius, $\rho = a_1/a_2$, allows for a very concise way to write the electric potential in each zone, (B.9-B.11).

$$\phi_1(r,\theta) = \sum_{\ell=0}^{\infty} \left[\frac{p_\ell^{(2)} + \rho^{2\ell+1}\left(p_\ell^{(3)} - p_\ell^{(2)}\right)}{a_1^{2\ell+1}}\, r^\ell - r\, E_0\, \delta_{\ell,1}\right] P_\ell(\cos\theta) \tag{B.9}$$

$$\phi_2(r,\theta) = \sum_{\ell=0}^{\infty} \left[\frac{p_\ell^{(3)} - p_\ell^{(2)}}{a_2^{2\ell+1}}\, r^\ell + \frac{p_\ell^{(2)}}{r^{\ell+1}} - r\, E_0\, \delta_{\ell,1}\right] P_l(\cos\theta) \tag{B.10}$$

$$\phi_3(r,\theta) = \sum_{\ell=0}^{\infty} \left[\frac{p_\ell^{(3)}}{r^{\ell+1}} - r\, E_0\, \delta_{\ell,1}\right] P_\ell(\cos\theta) \tag{B.11}$$

Combining these equations with eqn. B.1 provides the radial electric field in each region, $E_i^r(r,\theta)$. The radial continuity in the interface of $r = a_{1,2}$ leads to eqn. B.16, where ε_i is the electric permittivity of the i^{th} medium.

$$E_i^r(r,\theta) = -\frac{\partial\phi_i(r,\theta)}{\partial r} \tag{B.12}$$

$$E_1^r(r,\theta) = \sum_{\ell=0}^{\infty} \left[-\frac{p_\ell^{(2)} + \rho^{2l+1}\left(p_\ell^{(3)} - p_\ell^{(2)}\right)}{a_1^{2\ell+1}}\, \ell\, r^{\ell-1} + E_0\delta_{\ell,1}\right] P_\ell(\cos\theta) \tag{B.13}$$

$$E_2^r(r,\theta) = \sum_{\ell=0}^{\infty} \left[-\frac{p_\ell^{(3)} - p_\ell^{(2)}}{a_2^{2\ell+1}}\, \ell\, r^{\ell-1} + \frac{p_\ell^{(2)}}{r^{\ell+2}}\,(\ell+1) + E_0\delta_{\ell,1}\right] P_\ell(\cos\theta) \tag{B.14}$$

$$E_3^r(r,\theta) = \sum_{\ell=0}^{\infty} \left[\frac{p_\ell^{(3)}}{r^{\ell+2}}\,(\ell+1) + E_0\delta_{\ell,1}\right] P_\ell(\cos\theta) \tag{B.15}$$

$$\varepsilon_1\, E_1^r\,|_{r=a_1} = \varepsilon_2\, E_2^r\,|_{r=a_1} \tag{B.16}$$

$$\varepsilon_2\, E_2^r\,|_{r=a_2} = \varepsilon_3\, E_3^r\,|_{r=a_2} \tag{B.17}$$

So, substituting eqns. B.14, B.15 for the radial component of the electric field in each region into the field's radial continuity equation, eqn. B.17, resulted in eqn. B.18. Additionally, using eqns. B.13, B.14 with eqn. B.16 provides eqn. B.19.

$$p_\ell^{(3)} = a_2^{\ell+2}\frac{(\varepsilon_2-\varepsilon_3)[\ell\varepsilon_1+(\ell+1)\varepsilon_2] + \rho^{2\ell+1}(\varepsilon_1-\varepsilon_2)[\ell\varepsilon_3+(\ell+1)\varepsilon_2]}{[\ell\varepsilon_2+(\ell+1)\varepsilon_3][\ell\varepsilon_1-(\ell+1)\varepsilon_2] - \ell(\ell+1)\rho^{2\ell+1}(\varepsilon_1-\varepsilon_2)(\varepsilon_3-\varepsilon_2)}E_0\delta_{\ell,1} \tag{B.18}$$

$$p_\ell^{(2)} = \frac{a_1^{\ell+2}(\varepsilon_1-\varepsilon_2)E_0\delta_{\ell,1} - \ell\rho^{2\ell+1}(\varepsilon_1-\varepsilon_2)p_\ell^{(3)}}{\ell\varepsilon_1 - \ell\rho^{2\ell+1}(\varepsilon_1-\varepsilon_2) + (\ell+1)\varepsilon_2} \tag{B.19}$$

In both equations it becomes clear that the only ℓ modes that will be non-zero will be $\ell = 1$ (dipolar mode), since $\delta_{\ell,1}$ (the Kronecker Delta) appears multiplying every factor. Since there is only a dipolar term in the electric potential of region 3, eqn. B.20, and the electric potential of a dipole in vaccum can be written as eqn. B.21, [51] , when the dipole moment points in the z direction, it becomes clear that $p_1^{(3)}$ is directly proportional to the polarizability of region 3. This condition provides the equation for the polarizability of the outer region, α_3, eqn. B.22. This equation for the polarizability has a real and an imaginary component, since the electric permittivity of the metal and that of the outer medium have real and imaginary parts.

$$\phi_3(r,\theta) = \left(\frac{p_1^{(3)}}{r^2} - r\,E_0\right)\cos\theta \tag{B.20}$$

$$\phi_{dip}(r,\theta) = \frac{\hat{r}\cdot\boldsymbol{p}}{4\pi\varepsilon_0\varepsilon_3\,r^2} = \frac{p\,\cos\theta}{4\pi\varepsilon_0\varepsilon_3\,r^2} \tag{B.21}$$

$$\alpha_3^{SS} = \frac{p_1^{(3)}}{E_0} = 4\pi\varepsilon_0\,a_2^3\,\varepsilon_3\,\frac{(\varepsilon_2-\varepsilon_3)\,(\varepsilon_1+2\,\varepsilon_2) + \rho^3\,(\varepsilon_1-\varepsilon_2)\,(\varepsilon_3+2\,\varepsilon_2)}{(\varepsilon_2+2\varepsilon_3)\,(\varepsilon_1+2\varepsilon_2) + 2\rho^3\,(\varepsilon_1-\varepsilon_2)(\varepsilon_3-\varepsilon_2)} \tag{B.22}$$

An interesting property has risen from the fact that for $p_\ell^{(2,3)}$ the only mode that survives is the dipolar mode ($\ell = 1$), as shown in fig. B.2. By applying this to the equation for the electric potential inside the nanoshell, region 1, eqn. B.23 is obtained. With it, and eqn. B.1, the electric field in the inner region of the nanoshell is defined by eqn. B.24. Since $p_1^{(2,3)}$ are constants, it becomes clear that the field in said region is **uniform**! As a result of this, the active medium will **not** undergo the mode cascade that was the main concern in the nano-sphere model. [54]

$$\phi_1(r,\theta) = \frac{p_1^{(2)}+\rho^3(p_1^{(3)}-p_1^{(2)})}{a_1^3}r\,\cos\theta - r\,E_0\,\cos\theta \tag{B.23}$$

$$\boldsymbol{E}_1(r,\theta) = -\frac{\partial\phi_1}{\partial r}\hat{r} - \frac{1}{r}\frac{\partial\phi_1}{\partial\theta}\hat{\theta} = \left(E_0 - \frac{p_1^{(2)}+\rho^3(p_1^{(3)}-p_1^{(2)})}{a_1^3}\right)\hat{z} \tag{B.24}$$

Now! This is all very nice and accurate. However, this is the classical case and the steady state solution for a time dynamical system. Therefore, if the real, dynamical, system is to be solved, additional equations are needed, and quantum mechanics needs to be considered. The active molecules in the solution of region 1 will undergo excitation and, with it, spontaneous emission of radiation due to instabilities in the system as well as stimulated emission due to an external pump for the gain medium alone (not to be confused with the external driving field

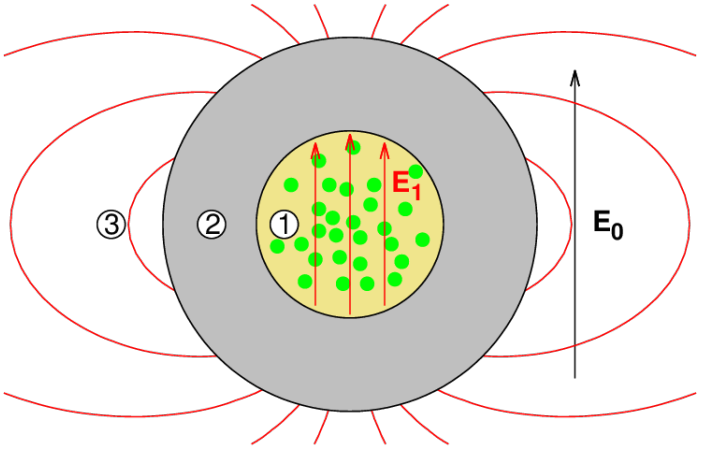

FIGURE B.2: Dipolar Mode for Nanoshell Geometry.

E_0). In order to consider the quantum mechanical side of this story, a two-level system will be considered.

Bibliography

[1] N. N. Initiative, "What is nanotechnology?." http://www.nano.gov/nanotech-101/what/definition, 09 2002.

[2] G. Binnig, H. Rohrer, C. Gerber, and E. Weibel, "Surface studies by scanning tunneling microscopy," *Physical Review Letters*, vol. 49, no. 1, pp. 57–61, 1982.

[3] C. E. Wieman and L. Hollberg, "Using diode lasers for atomic physics," *Review of Scientific Instruments*, vol. 62, pp. 1–20, 1 1991.

[4] H. W. Kroto, J. R. Heath, S. C. O'Brien, R. F. Curl, and R. E. Smalley, "C60: Buckminsterfullerene," *Nature*, vol. 318, pp. 162–163, 11 1985.

[5] G. A. Sotiriou and S. E. Pratsinis, "Antibacterial activity of nanosilver ions and particles," *Environmental Science and Technology*, vol. 44, no. 14, pp. 5649–5654, 2010. PMID: 20583805.

[6] K. Park, "Nanotechnology: What it can do for drug delivery," *Journal of controlled release : official journal of the Controlled Release Society*, vol. 120, pp. 1–3, 07 2007.

[7] A. G. Cuenca, H. Jiang, S. N. Hochwald, M. Delano, W. G. Cance, and S. R. Grobmyer, "Emerging implications of nanotechnology on cancer diagnostics and therapeutics," *Cancer*, vol. 107, no. 3, pp. 459–466, 2006.

[8] I. K. Herrmann, M. Urner, F. M. Koehler, M. Hasler, B. Roth-Z'Graggen, R. N. Grass, U. Ziegler, B. Beck-Schimmer, and W. J. Stark, "Blood purification using functionalized core/shell nanomagnets," *Small*, vol. 6, no. 13, pp. 1388–1392, 2010.

[9] T. Dürkop, S. A. Getty, E. Cobas, , and M. S. Fuhrer, "Extraordinary mobility in semiconducting carbon nanotubes," *Nano Letters*, vol. 4, no. 1, pp. 35–39, 2004.

[10] J. He, H. Lou, L. Zhang, and M. Chan, *Silicon-Based Nanowire MOSFETs: From Process and Device Physics to Simulation and Modeling*. INTECH Open Access Publisher, 2011.

[11] A. S. Arnold, J. S. Wilson, M. G. Boshier, and J. Smith, "A simple extended-cavity diode laser," *Review of Scientific Instruments*, vol. 69, pp. 1236–1239, 3 1998.

[12] J. L. O'Brien, "Optical quantum computing," *Science*, vol. 318, pp. 1567–1570, 12 2007.

[13] J. Bao and M. G. Bawendi, "A colloidal quantum dot spectrometer," *Nature*, vol. 523, pp. 67–70, 07 2015.

[14] A. Fert, "Nobel lecture: Origin, development, and future of spintronics," *Reviews of Modern Physics*, vol. 80, no. 4, pp. 1517–1530, 2008.

[15] P. Saunders and N. Zhedulev, "Metamaterials: The next photonics revolution." Video, October 2009.

[16] S. Maier, *Plasmonics: Fundamentals and Applications*. Springer US, 2010.

[17] L. Novotny and B. Hecht, *Principles of Nano-Optics*. Cambridge University Press, 2006.

[18] H. A. Atwater and A. Polman, "Plasmonics for improved photovoltaic devices," *Nat Mater*, vol. 9, pp. 205–213, 03 2010.

[19] N. Fang, H. Lee, C. Sun, and X. Zhang, "Sub-diffraction-limited optical imaging with a silver superlens," *Science*, vol. 308, no. 5721, pp. 534–537, 2005.

[20] R. B. Nielsen, M. D. Thoreson, W. Chen, A. Kristensen, J. M. Hvam, V. M. Shalaev, and A. Boltasseva, "Toward superlensing with metal–dielectric composites and multilayers," *Applied Physics B*, vol. 100, no. 1, pp. 93–100, 2010.

[21] F. Capolino, *Theory and Phenomena of Metamaterials*. Metamaterials Handbook, CRC Press, 2009.

[22] I. Suarez, E. Fitrakis, P. Rodriguez-Canto, R. Abargues, I. Tomkos, and J. Martinez-Pastor, "Surface plasmon-polariton amplifiers," in *Transparent Optical Networks (ICTON), 2012 14th International Conference on*, pp. 1–5, IEEE, 2012.

[23] J. C. M. Garnett, "Colours in metal glasses and in metallic films," *Philosophical Transactions of the Royal Society of London A: Mathematical, Physical and Engineering Sciences*, vol. 203, no. 359-371, pp. 385–420, 1904.

[24] F. Currell and S. McMahon, *Gold Nanoparticles for Imaging and Radiotherapy*, pp. 65–92. Elsevier, 2013.

[25] I. Freestone, N. Meeks, M. Sax, and C. Higgitt, "The lycurgus cup —a roman nanotechnology," *Gold Bulletin*, vol. 40, no. 4, pp. 270–277, 2007.

[26] D. J. Bergman and M. I. Stockman, "Surface plasmon amplification by stimulated emission of radiation: quantum generation of coherent surface plasmons in nanosystems," *Physical review letters*, vol. 90, no. 2, p. 027402, 2003.

[27] N. I. Zheludev, S. Prosvirnin, N. Papasimakis, and V. Fedotov, "Lasing spaser," *Nature Photonics*, vol. 2, no. 6, pp. 351–354, 2008.

[28] M. I. Stockman, "Spasers explained," *Nature Photonics*, vol. 2, pp. 327–329, 06 2008.

[29] E. Abbe, *Gesammelte Abhandlungen*. No. v. 2 in Gesammelte Abhandlungen, Gustav Fischer, 1906.

[30] editorial, "Beyond the diffraction limit," *Nat Photon*, vol. 3, pp. 361–361, 07 2009.

[31] T. A. Klar and S. W. Hell, "Subdiffraction resolution in far-field fluorescence microscopy," *Opt. Lett.*, vol. 24, pp. 954–956, Jul 1999.

[32] Y. Choi", "Overcoming the diffraction limit using multiple light scattering in a highly disordered medium," *Physical Review Letters*, vol. 107, no. 2, 2011.

[33] S. Kawata, Y. Inouye, and P. Verma, "Plasmonics for near-field nano-imaging and superlensing," *Nat Photon*, vol. 3, pp. 388–394, 07 2009.

[34] J. Polo, T. Mackay, and A. Lakhtakia, *Electromagnetic surface waves: a modern perspective*. Newnes, 2013.

[35] B. Hecht, B. Sick, U. P. Wild, V. Deckert, R. Zenobi, O. J. Martin, and D. W. Pohl, "Scanning near-field optical microscopy with aperture probes: Fundamentals and applications," *The Journal of Chemical Physics*, vol. 112, no. 18, pp. 7761–7774, 2000.

[36] W. Denk, J. Strickler, and W. Webb, "Two-photon laser scanning fluorescence microscopy," *Science*, vol. 248, no. 4951, pp. 73–76, 1990.

[37] M. L. Brongersma and P. G. Kik, "Surface plasmon nanophotonics," *Springer series in optical sciences*, vol. 131, p. 1, 2007.

[38] D. Bohm and D. Pines, "A collective description of electron interactions: Iii. coulomb interactions in a degenerate electron gas," *Physical Review*, vol. 92, no. 3, p. 609, 1953.

[39] D. Pines, "A collective description of electron interactions: Iv. electron interaction in metals," *Physical Review*, vol. 92, no. 3, p. 626, 1953.

[40] D. Pines, "Collective energy losses in solids," *Reviews of Modern Physics*, vol. 28, no. 3, p. 184, 1956.

[41] R. Ritchie, "Plasma losses by fast electrons in thin films," *Physical Review*, vol. 106, no. 5, p. 874, 1957.

[42] J. Hopfield, "Theory of the contribution of excitons to the complex dielectric constant of crystals," *Physical Review*, vol. 112, no. 5, p. 1555, 1958.

[43] M. Pelton and G. W. Bryant, *Introduction to metal-nanoparticle plasmonics*, vol. 5. John Wiley & Sons, 2013.

[44] J. Brambring and H. Raether, "Plasma radiation from thin silver foils excited by light," *Physical Review Letters*, vol. 15, no. 23, p. 882, 1965.

[45] E. Kretschmann and H. Raether, "Radiative decay of non radiative surface plasmons excited by light," *Zeitschrift für Naturforschung A*, vol. 23, no. 12, pp. 2135–2136, 1968.

[46] A. Otto, "Excitation of nonradiative surface plasma waves in silver by the method of frustrated total reflection," *Zeitschrift für Physik*, vol. 216, no. 4, pp. 398–410, 1968.

[47] T. W. Ebbesen, H. J. Lezec, H. F. Ghaemi, T. Thio, and P. A. Wolff, "Extraordinary optical transmission through sub-wavelength hole arrays," *Nature*, vol. 391, pp. 667–669, 02 1998.

[48] J. B. Pendry, "Negative refraction makes a perfect lens," *Phys. Rev. Lett.*, vol. 85, pp. 3966–3969, Oct 2000.

[49] U. Kreibig and P. Zacharias, "Surface plasma resonances in small spherical silver and gold particles," *Zeitschrift für Physik*, vol. 231, no. 2, pp. 128–143, 1970.

[50] J. Jackson, *Classical Electrodynamics*. Wiley, 1998.

[51] J. D. Griffiths, *Introduction to Electrodynamics*. Pearson Education, 2014.

[52] K. Y. Kim, "Plasmonics-principles and applications," *Application of Surface Plasmon Resonance Based Metal Nanoparticles*, 2012.

[53] G. Mie and H. Van de Hulst, "Light scattering by small particles," *Ann. Phys*, vol. 25, p. 377, 1908.

[54] A. Veltri and A. Aradian, "Optical response of a metallic nanoparticle immersed in a medium with optical gain," *Physical Review B*, vol. 85, no. 11, 2012.

[55] A. Sudarkin and P. Demkovich, "Excitation of surface electromagnetic waves on the boundary of a metal with an amplifying medium," *Sov. Phys. Tech. Phys*, vol. 34, no. 764766, p. 57, 1989.

[56] V. Rivera, O. Silva, Y. Ledemi, Y. Messaddeq, and E. Marega Jr, *Collective Plasmon-Modes in Gain Media: Quantum Emitters and Plasmonic Nanostructures*. Springer, 2014.

[57] V. Rivera, Y. Ledemi, S. Osorio, F. Ferri, Y. Messaddeq, L. Nunes, and E. Marega, "Optical gain medium for plasmonic devices," in *SPIE OPTO*, pp. 86211J–86211J, International Society for Optics and Photonics, 2013.

[58] M. P. Nezhad, K. Tetz, and Y. Fainman, "Gain assisted propagation of surface plasmon polaritons on planar metallic waveguides," *Optics Express*, vol. 12, no. 17, pp. 4072–4079, 2004.

[59] S. A. Maier, "Gain-assisted propagation of electromagnetic energy in subwavelength surface plasmon polariton gap waveguides," *Optics Communications*, vol. 258, no. 2, pp. 295 – 299, 2006.

[60] M. Noginov, V. A. Podolskiy, G. Zhu, M. Mayy, M. Bahoura, J. Adegoke, B. Ritzo, and K. Reynolds, "Compensation of loss in propagating surface plasmon polariton by gain in adjacent dielectric medium," *Optics express*, vol. 16, no. 2, pp. 1385–1392, 2008.

[61] C. Van Vlack, P. T. Kristensen, and S. Hughes, "Spontaneous emission spectra and quantum light-matter interactions from a strongly coupled quantum dot metal-nanoparticle system," *Physical Review B*, vol. 85, no. 7, p. 075303, 2012.

[62] A. De Luca, M. P. Grzelczak, I. Pastoriza-Santos, L. M. Liz-Marzán, M. La Deda, M. Striccoli, and G. Strangi, "Dispersed and encapsulated gain medium in plasmonic nanoparticles: a multipronged approach to mitigate optical losses," *ACS nano*, vol. 5, no. 7, pp. 5823–5829, 2011.

[63] A. Fang, T. Koschny, M. Wegener, and C. Soukoulis, "Self-consistent calculation of metamaterials with gain," *Physical Review B*, vol. 79, no. 24, p. 241104, 2009.

[64] L. Lugiato, F. Prati, and M. Brambilla, *Nonlinear optical systems*. Cambridge University Press, 2015.

[65] N. W. Ashcroft and N. D. Mermin, "Solid state physics," *Saunders, Philadelphia*, vol. 293, 1976.

[66] J. S. Yang, S. G. Lee, S.-G. Park, E.-H. Lee, *et al.*, "Drude model for the optical properties of a nano-scale thin metal film revisted," *Journal of the Korean Physical Society*, vol. 55, no. 6, pp. 2552–2555, 2009.

[67] J. C. Kah, N. Phonthammachai, R. C. Wan, J. Song, T. White, S. Mhaisalkar, I. Ahmadb, C. Shepparda, and M. Olivoc, "Synthesis of gold nanoshells based on the deposition-precipitation process," *Gold Bulletin*, vol. 41, no. 1, pp. 23–36, 2008.

[68] A. M. Brito-Silva, R. G. Sobral-Filho, R. Barbosa-Silva, C. B. de Araújo, A. Galembeck, and A. G. Brolo, "Improved synthesis of gold and silver nanoshells," *Langmuir*, vol. 29, no. 13, pp. 4366–4372, 2013.

[69] S. Duraiswamy and S. A. Khan, "Plasmonic nanoshell synthesis in microfluidic composite foams," *Nano letters*, vol. 10, no. 9, pp. 3757–3763, 2010.

[70] S. Kalele, S. Gosavi, J. Urban, and S. Kulkarni, "Nanoshell particles: synthesis, properties and applications," *Current Science*, vol. 91, no. 8, pp. 1038–1052, 2006.

[71] A. Jenkins, "Self-oscillation," *Physics Reports*, vol. 525, no. 2, pp. 167–222, 2013.

[72] M. Sargent III, M. Scully, and W. Lamb Jr, "Laser physics," 1974.

[73] P. B. Johnson and R.-W. Christy, "Optical constants of the noble metals," *Physical review B*, vol. 6, no. 12, p. 4370, 1972.

[74] A. L. Feng, M. L. You, L. Tian, S. Singamaneni, M. Liu, Z. Duan, T. J. Lu, F. Xu, and M. Lin, "Distance-dependent plasmon-enhanced fluorescence of upconversion nanoparticles using polyelectrolyte multilayers as tunable spacers," *Scientific reports*, vol. 5, 2015.

[75] E. I. Galanzha, R. Weingold, D. A. Nedosekin, M. Sarimollaoglu, A. S. Kuchyanov, R. G. Parkhomenko, A. I. Plekhanov, M. I. Stockman, and V. P. Zharov, "Spaser as novel versatile biomedical tool," *arXiv preprint arXiv:1501.00342*, 2015.

[76] M. I. Stockman, "The spaser as a nanoscale quantum generator and ultrafast amplifier," *Journal of Optics*, vol. 12, no. 2, p. 024004, 2010.

[77] D. V. Voronine, W. Huo, and M. Scully, "Ultrafast dynamics of surface plasmon nanolasers with quantum coherence and external plasmonic feedback," *Journal of Optics*, vol. 16, no. 11, p. 114013, 2014.

[78] M. Noginov, G. Zhu, A. Belgrave, R. Bakker, V. Shalaev, E. Narimanov, S. Stout, E. Herz, T. Suteewong, and U. Wiesner, "Demonstration of a spaser-based nanolaser," *Nature*, vol. 460, no. 7259, pp. 1110–1112, 2009.

[79] M. Noginov, G. Zhu, M. Bahoura, J. Adegoke, C. Small, B. Ritzo, V. Drachev, and V. Shalaev, "Enhancement of surface plasmons in an ag aggregate by optical gain in a dielectric medium," *Optics letters*, vol. 31, no. 20, pp. 3022–3024, 2006.

[80] E. B. Dickerson, E. C. Dreaden, X. Huang, I. H. El-Sayed, H. Chu, S. Pushpanketh, J. F. McDonald, and M. A. El-Sayed, "Gold nanorod assisted near-infrared plasmonic photothermal therapy (pptt) of squamous cell carcinoma in mice," *Cancer letters*, vol. 269, no. 1, pp. 57–66, 2008.

[81] G. T. Purves, *Absorbtion and dispersion in atomic vapours: Applications to interferometry*. PhD thesis, Durham University, http://etheses.dur.ac.uk/2663/, 2006.

[82] C. Tang, *Fundamentals of Quantum Mechanics: For Solid State Electronics and Optics*. Cambridge University Press, 2009.